2015

A STUDY TO EVALUATE NON-UNIFORM PHASE MAPS IN SHAPE MEMORY ALLOYS USING FINITE ELEMENT METHOD

Naren Motte

A STUDY TO EVALUATE NON-UNIFORM PHASE MAPS IN SHAPE MEMORY ALLOYS USING FINITE ELEMENT METHOD

A thesis submitted in partial fulfilment of the requirements for the degree of

Master of Science in Mechanical & Nuclear Engineering at

Virginia Commonwealth University.

by

NAREN MOTTE

B.S. Mechanical Engineering – JNTU, India – 2010

Director: Dr. Ibrahim Guven

Assistant Professor, Department of Mechanical and Nuclear Engineering

Department of Mechanical & Nuclear Engineering

Virginia Commonwealth University

Richmond, Virginia

August, 2015

Acknowledgements

First, I would like to express my sincere gratitude to my advisor Dr. Ibrahim Guven who has supported me with his patience, guidance and expertise. I couldn't accomplish my present achievements without his supports and motivation. I highly appreciate his vast knowledge in the area, his assistance in all levels of my research.

Besides, I would like to sincerely thank Dr. Sama Bilbao y León and Dr. Karla M. Mossi for their support in my initial days in VCU. My special thanks to Dr. Ümit Özgür whose presence on the thesis committee is highly appreciated. My heart full thanks go to the Department of the Mechanical and Nuclear Engineering for supporting me throughout my studies.

Many thanks to the friends from the Mechanical and Nuclear Engineering department, namely: Ganesh, Keith, Sanjay, Naveen, Brandon, Noel, Ahmed and Dalsung.

Special thanks got to my friends in Richmond, namely: Vinay, Shruthi, Rahul, Bhanu, Naina, Venkatesh, Karthik and many others I am sure I have forgotten to name.

Last but not the least; I would like to thank my Creator and the two people chosen by him to protect and guide me in my youth, my parents, whom I missed so much, for their lifelong indescribable support, patience and love.

Table of Contents

Page

List of Tables

Page

List of Figures

Page

Abstract

A STUDY TO EVALUATE NON-UNIFORM PHASE MAPS IN SHAPE MEMORY ALLOYS USING FINITE ELEMENT METHOD

By Naren Motte

A thesis submitted in partial fulfillment of the requirements for the degree of

Master of Science in Mechanical & Nuclear Engineering at

Virginia Commonwealth University.

Virginia Commonwealth University,
[2015]

Major Director: Dr. Ibrahim Guven
Assistant Professor, Department of Mechanical and Nuclear Engineering
Department of Mechanical & Nuclear Engineering

The unique thermo-mechanical behavior of Shape Memory Alloys (SMAs), such as their ability to recover the original shape upon heating or being able to tolerate large deformations without undergoing plastic transformations, makes them a good choice for actuators.

This work studies their application in the aerospace and defense industries where SMA components can serve as release mechanisms for gates of enclosures that have to be deployed remotely. This work provides a novel approach in evaluating the stress and heat induced change of phase in a SMA, in terms of the transformation strain tensor. In particular, the FEA tool

ANSYS has been used to perform a 2-D analysis of a Cu-Al-Zn-Mn SMA specimen undergoing a nontraditional loading path in two steps with stress and heating loads. In the first load step, tensile displacement is applied, followed by the second load step in which the specimen is heated while the end displacements are held constant.

A number of geometric configurations are examined under the two step loading path. Strain results are used to calculate transformation strain which provides a quantitative measure of phase at a material point; when transformation strain is zero, the material point is either twinned martensite, or austenite depending on the temperature. Transformation strain value of unity corresponds to detwinned martensite. A value between zero and one indicates mixed phase.

In this study, through two step loading in conjunction with transformation strain calculations, a method for mapping transient non-uniform distribution of phases in an SMA is introduced.

Ability to obtain drastically different phase distributions under same loading path by modifying the geometry is demonstrated. The failure behavior of SMAs can be designed such that the load level the crack initiates and the path it propagates can be customized.

CHAPTER 1 Introduction to Shape Memory Alloys

1.1 Introduction

Alloying, smelting and forging of traditional metals have been used for centuries. Much great advancement has taken place in the field of material science owing to the deep understanding of material behavior and microstructure. In the recent years, there has been interesting interest in the use of "smart materials". These materials are lighter in weight and yet stronger with desired materials properties. They tend to exhibit mechanical response in a controlled fashion to external stimuli such as temperature, stress, electric or magnetic fields. For example, when an electrical current is passed through a piezoelectric material, we observe a significant increase in size. Such a mechanical response is more in order of magnitude for the smart materials than when compared to the mechanical response of traditional metals [1]. Shape memory alloys (SMAs), magnetostrictive materials, electrostrictive materials, piezoelectric materials and piezomagnetic materials could be listed as some of the examples for smart materials.

Ability to remember its original shape after general deformations, gives the name "Shape Memory" for SMAs. When loaded at lower temperatures, the material deforms and after removal of the load, the material stays deformed. When heated to certain temperatures it returns to its original dimensions [1]. To understand this behavior one must understand the micro structure of the alloy. This unique behavior is due to the existence of two material phases, austenite and martensite. These phases have different crystal structures as shown in Figure 1.1; the austenite phase exists in cubic structure, while the martensite is in tetragonal, orthorhombic or monoclinic structures. The martensite structure of SMA is a rather flexible and elongated. After application of stress, the distance between atoms alters causing twist in the crystal structure of the alloy. When heated to certain temperature it is promoted to the austenite phase. At this time, the crystal

structure of the alloy becomes a stable body-centered cubic. The distance between atoms returns to its original value, and the alloy restores its original shape. These distinct molecular structures lead to drastically different properties.

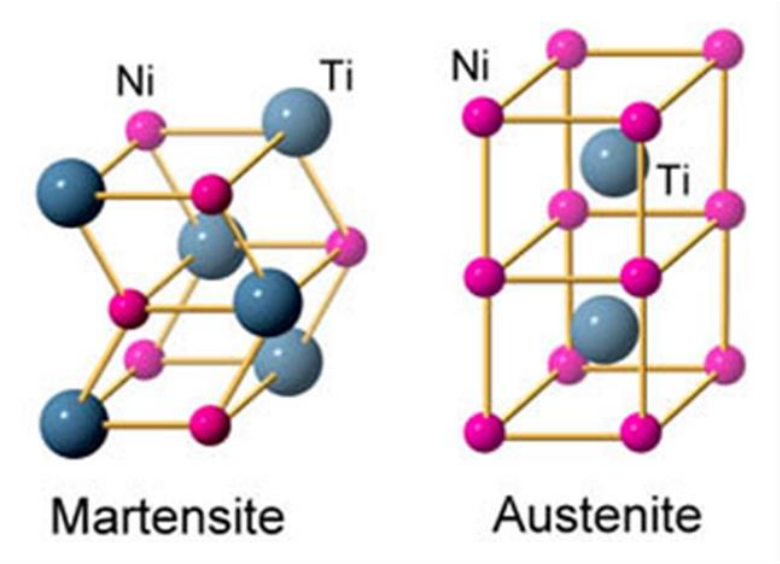

Figure 1.1: Crystal structures of martensite and austenite phases [2].

1.2 Brief History of Shape Memory Alloys

The major milestone in the discovery of SMAs was established with the discovery of martensite in steel in the late 1890s by Adolf Martens. By the year 1949, Kurdjumov and Khandros conducted experiments on CuZn and CuAl alloys [3]. Based on these studies, the concept of thermoelastic martensitic transformation was proved. A breakthrough occurred when Buehler and his associates studied and aided to the development of NiTi alloy. The name NiTi was combined with NOL at the end in the honor of being discovered at the Naval Ordinance Laboratory (NOL) and hence the term "NiTiNOL" was given to the material [4]. By 1965, studies show that with the addition of third alloying element the SMA transformation temperatures can be varied [5]. Cryofit marked the beginning of active research in commercial sector, with the F-14 fighter aircrafts made use of SMA for pipe coupling [6]. Continued research in different applications led to the high temperature SMAs (HTSMA) such as TiAu, TiPt and TiPd, magnetic SMAs and shape memory polymers.

1.3 Phase Transformation in SMAs

The phase diagram of a metal depicts different phases present in an alloy as a function of temperature; the phases are separated by phase boundaries. The percentage concentration of different alloying metals in an alloy is a very important factor and this is represented in the x-axis of a phase transformation diagram and the y-axis depicts other variables like stress or temperature shown in Figure 1.2.

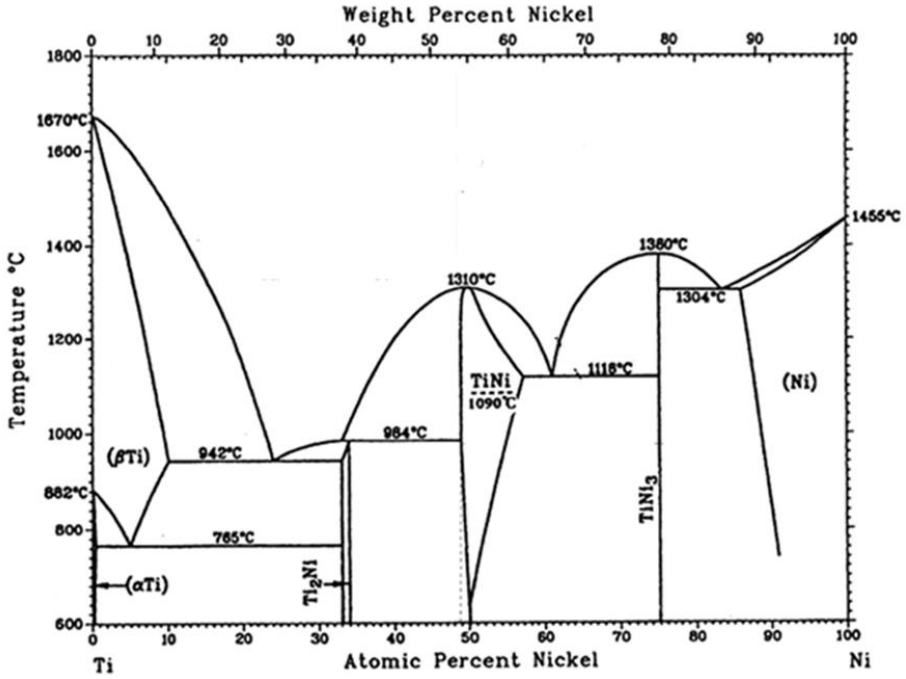

Figure 1.2: Phase diagram of NiTi alloy [7].

At a specific composition of alloy concentration, stress and temperature variables are used to establish the phases for an alloy. The transformation from austenite to martensite is a diffusionless phase transformation, in which atoms move due to the shear lattice distortion [1], this transformation is known as martensitic transformation. Each martensitic crystal formed can have a different orientation direction, called a variant. The assembly of martensitic variants can exist in two forms: twinned martensite and detwinned martensite. Figure 1.3 describes the phase transformation of austenite to twinned martensite to detwinned martensite.

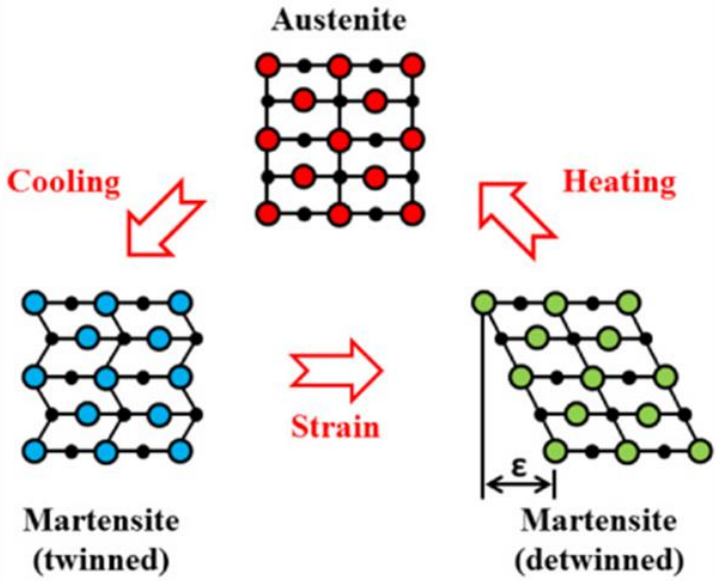

Figure 1.3: Transformation of austenite to twinned martensite to detwinned martensite [4].

Austenite is the parent phase in SMA and the transition from austenite to martensite is known as forward transformation. This transformation takes place when the material is cooled to lower temperature. Now, if the same material is heated the material transforms back to austenite, this transformation is known as reverse transformation. The phase transformation can be induced either by a temperature change or by applying stress.

1.3.1 Phase Transformation with Change in Temperature

The phase transformation in SMAs is associated with four particular temperatures [1]. Initially, material is considered to be in austenite phase at stress free state. Incidentally, when the material is cooled down, the temperature first hits martensite start temperature (M_s) the martensite phase starts leading to a mixture of austenite and martensite.

When the material is further cooled, the temperature reaches martensite finish temperature (M_f) the phase of the material is completely twinned martensite. When austenite is transformed to twinned martensite, the martensite formed occurs by twinning and the twins arrange themselves to minimize overall strain energy due to transformation, thus there is no shape change.

Similarly, when the same material in twinned martensite phase is heated, the temperature first hits austenite start temperature (A_s), which marks the beginning of austenite phase. When the

temperature is further increased, the temperature initiates austenite finish temperature (A_f), and this is where the material is complete austenite. Figure 1.4 gives a schematics of phase transformations at M_s, M_f, A_s and A_f temperatures.

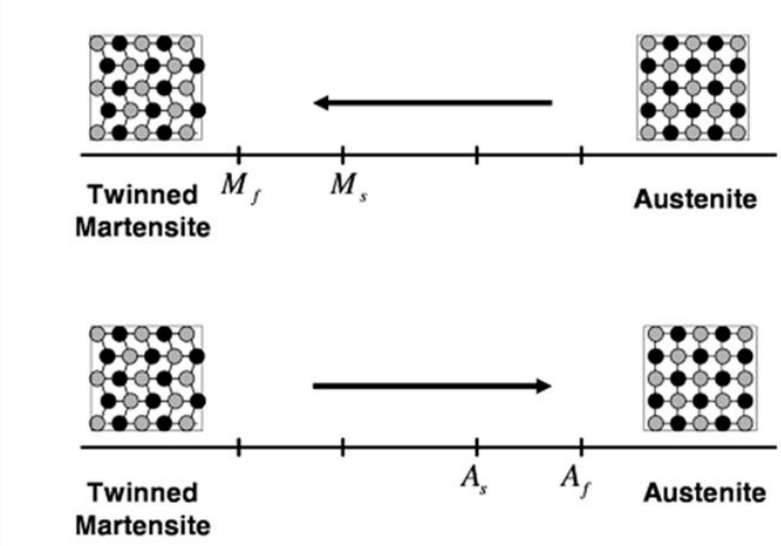

Figure 1.4: Transformation of material phase at M_s, M_f, A_s, A_f [1].

1.3.2 Phase Transformation with Change in Stress

When SMA is mechanically loaded at temperature below M_s, (at this temperature the material is in twinned martensite phase) at a certain stress it transforms into detwinned martensite. The minimum stress required to detwin the variants in martensite is known as the detwinning start stress (σ_s) and the minimum stress at which the material is completely detwinned is known as detwinning finish stress (σ_f). Figure 1.5 depicts detwinning start stress and finish stress in a phase transformation diagram.

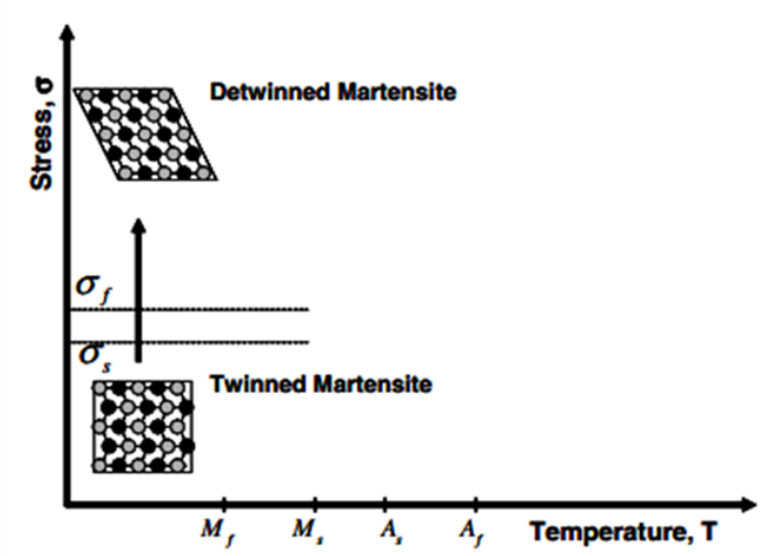

Figure 1.5: Transformation of material phase from twinned to detwinned martensite [1].

At this stage the material is mechanically deformed and is in detwinned phase. The phase transition results in austenite when heated to a temperature greater than A_f, and in this process, the original shape is recovered. This phase transformation takes place across four new transformation temperatures (M_f^σ, M_S^σ, A_S^σ, A_f^σ), shown in Figure 1.6 [1]. These transformation temperatures depend on the magnitude of the load, as the load increases these temperatures increases. When the material phase is austenite, and it is loaded greater than σ_f the material transforms into detwinned martensite with macroscopic deformation.

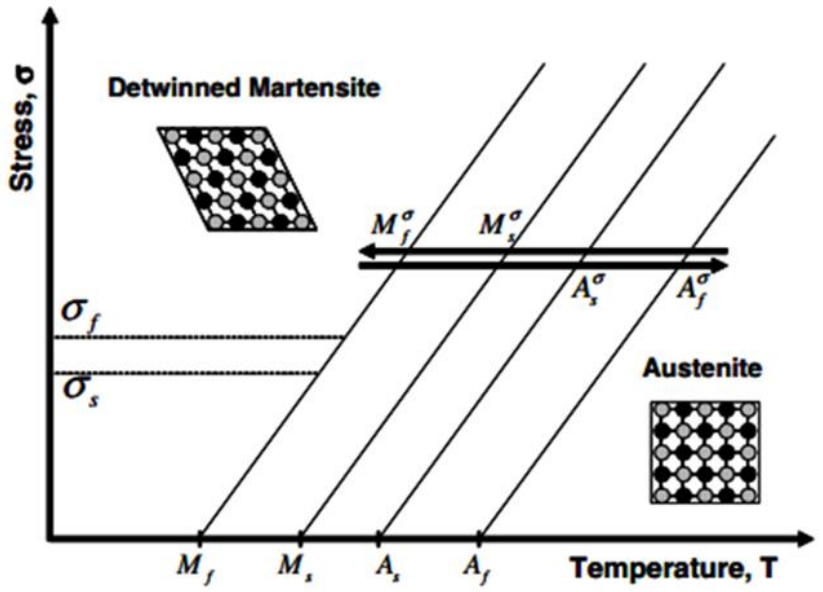

Figure 1.6: Transformation of material phase from Detwinned martensite to austenite [1].

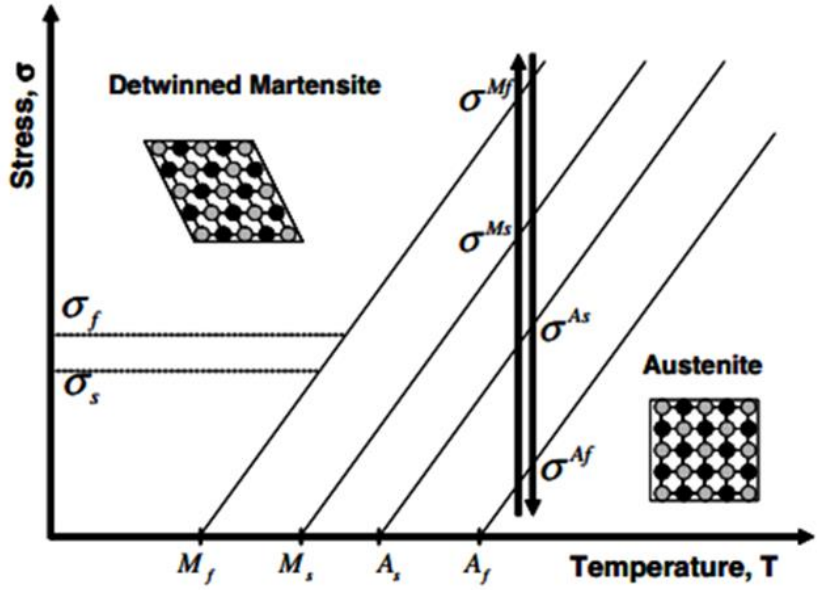

Figure 1.7: Transformation of material phase from austenite to detwinned martensite [1].

The minimum stress at which martensite phase starts is σ^{Ms} and the stress at which the material transforms into complete martensite is σ^{Mf}. When the material is unloaded it comes back to austenite phase with complete shape recovery. During unloading the austenite phase starts at

stress σ^{As} and as the stress reaches σ^{Af} the material is complete austenite. This process is described in Figure 1.7.

1.4 Superelasticity in SMAs

The stress induced transformation which generates strain during loading is called superelasticity, and this strain is recovered upon unloading [1]. The material is stable in the austenite phase at any temperature greater than A_f. This austenite phase would have to undergo elastic loading when high stress is applied. The martensite phase starts at a particular stress σ^{Ms}, which is described in Figure 1.8. Such a phenomenon can be observed with the change in slope on the stress-strain diagram. The material further converts to a complete detwinned martensite, at stress σ^{Mf}. It can be observed in the stress-strain diagram the completion of transformation with the change in slope on the end of this transformation. Even with further increase in the stress at this point, there is no change in the phase transformation.

Now, when it is unloaded, the stress intersects σ^{As} where the austenite phase starts. The shape which has been deformed starts to recover at this point. When unloaded further, the unloading path intersects austenite finish stress σ^{Af}, where a total shape recovery is achieved and the material is complete austenite. "Superelasticity" or "Pseudo-elasticity" would describe this process of recovering a deformed shape. In the above stress-strain plot Figure 1.8, a phase transformation can be identified with the change in the slope of the hysteresis. Hysteresis defines the amount of energy dissipated in the transformation cycle.

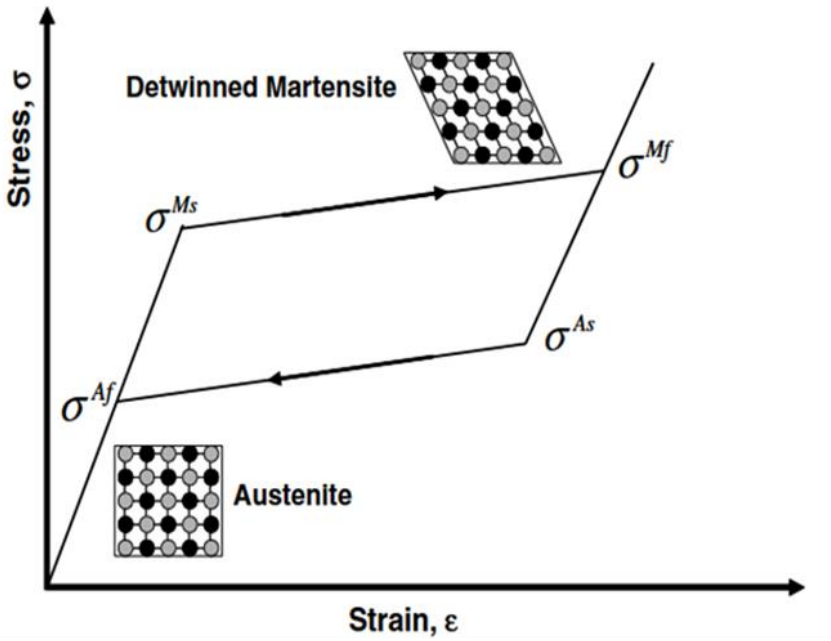

Figure 1.8: Superelastic behaviour of SMA [1]

1.5 Shape Memory Effect (SME) in SMAs

A unique feature of the SMAs is the shape memory effect (SME). Starting from point A, initially the material is in austenite phase shown in the Figure 1.9. When the material is cooled below the M_f temperature, the twinned martensite is formed at point B. At this point, if the material is loaded at the same temperature, the stress reaches stress σ_s where the detwinning of martensite starts. Further loading will lead to stress σ_f where the crystal transforms to complete detwinned martensite. With further loading the material stays in detwinned martensite state and point C is reached. The completion of transformation can be observed with the change in the slope. The material is mechanically deformed at this point and when the load is removed the material remains deformed can be represented by point D.

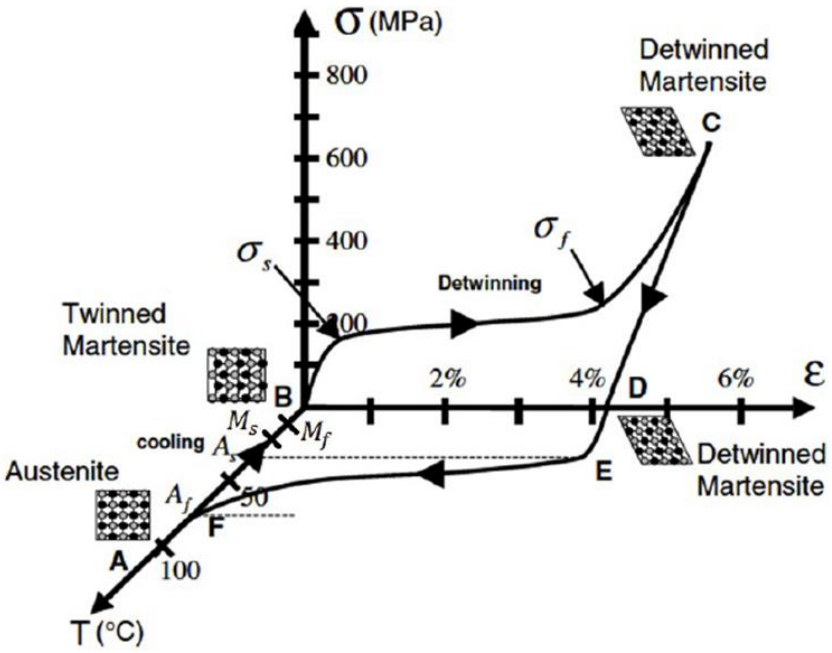

Figure 1.9: Shape memory effect of SMA [1]

At point D, when the material is heated it reaches point E where the temperature passes the austenite start temperature (A_s). At this point the shape recovery of the material starts, when it is further heated austenite finish temperature (A_f) is initiated at point F where the material is now complete austenite and the total shape is recovered. This phenomenon is called the sme [1], which is shown in Figure 1.9. The strain recovered in this transformation from detwinned martensite to austenite at point D is termed as the transformation strain (ε_t).

1.6 Application of SMAs

Due to the unique properties discussed so far the SMAs have gained much attention in different fields.

1.6.1 Aerospace Applications

The use of SMAs in the aerospace field has first started with Smart Wing program and Smart Aircraft and Marine Propulsion System demonstration (SAMPSON) program [8]. Wire tendons in the form of torque tubes make use of SMAs. The wire tendons were used to actuate hingeless ailerons and the torque tube was used that initiated span wise wing twist of F-18 aircraft wing, shown in Figure 1.10.

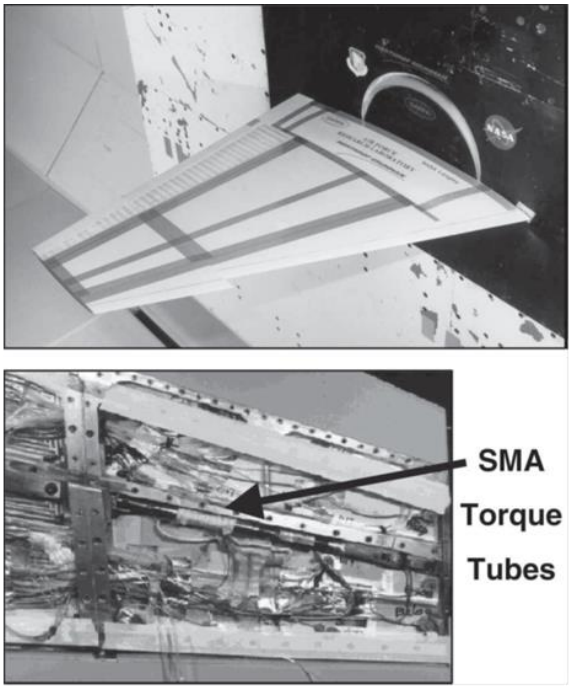

Figure 1.10: SMA torque tubes [8]

Some Boeing aircraft makes use of the SMAs to reduce the engine noise during takeoff and landing [8]. Chevrons are part of the engine exit which helps with mixing of flow of exhaust gases and reduce engine noise. On the top of the chevrons the SMA beams are fabricated. At the low speeds, the SMA is bent with the application of heat which contracts the chevron. Likewise, at high velocities the SMA is cooled into martensite and thus straightening the chevron. Along with decreasing the noise it also increases the engine performance [8]. Figure 1.11 shows the SMA beams fabricated to the chevrons.

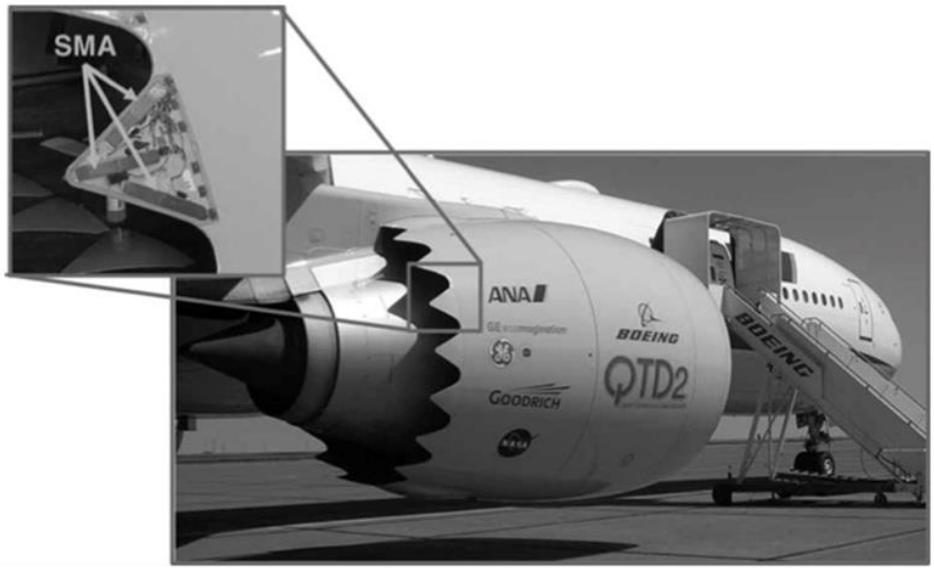

Figure 1.11: SMA beams as chevrons [8]

At zero atmosphere environments in space applications SMAs are used for low shock release application, actuation and vibration damping [8]. Devices like Qwknut and the micro set-nut are developed which use SMAs for the vibration damping application. In order to rotate solar panels installed in a satellite, SMAs in the form of thin strips is used in actuators.

1.6.2 Medical Applications

SMAs make promising material in medical applications since,

i. They don't oxidize in contact with blood and thus they can be used inside the body.
ii. They are hypo-allergic when comes in contact with the body.

The SMAs are used in the form of orthodontic wires, which are used in dental braces shown in Figure 1.12. The SMA wire uses superelasticity property in this application. Initially, the orthodontic wire is in austenite phase. During the insertion of the braces, the wire is deformed due to which the material phase converts to detwinned martensite [9]. Once the braces are positioned properly, the material tries to go back to austenite phase this process of going back to its original phase helps the brackets hold the teeth tightly.

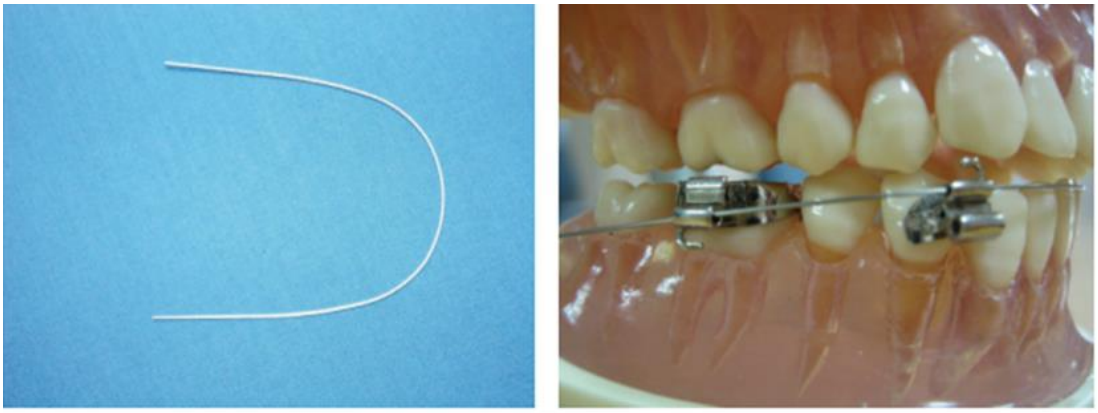

Figure 1.12: SMA orthodontic wire as dental braces [9]

In the endodontic field, root canal surgery is an important area. The endodontic file is used for the root canal surgeries. The device is mainly used for cleaning and shaping of tooth. This process induces a large strain on the file, which uses the superelasticity property to recover from the deformation [9].

Figure 1.13: SMA endodontic file [9]

SMA's are used to make Simon filter, a cardiovascular device used to filter the clots which are travelling in the blood vessels [11]. This device works on the principle of shape memory effect. Figure 1.14 shows the original shape of the filter, to insert it into the body the device is deformed and placed on a catheter tip shown in Figure 1.15.

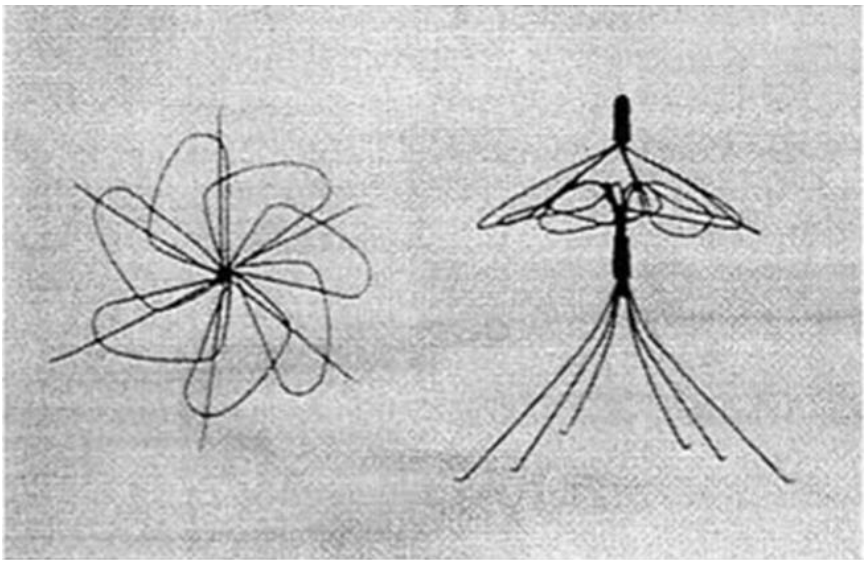

Figure 1.14: Simon filter [11]

While inserting the filter inside the body, a saline solution flowing through the catheter is used as a coolant to keep the filter in lower temperature. When the catheter releases the filter, the flow of the saline solution is stopped. Due to the body temperature, the filter is heated and shape recovery takes place [10].

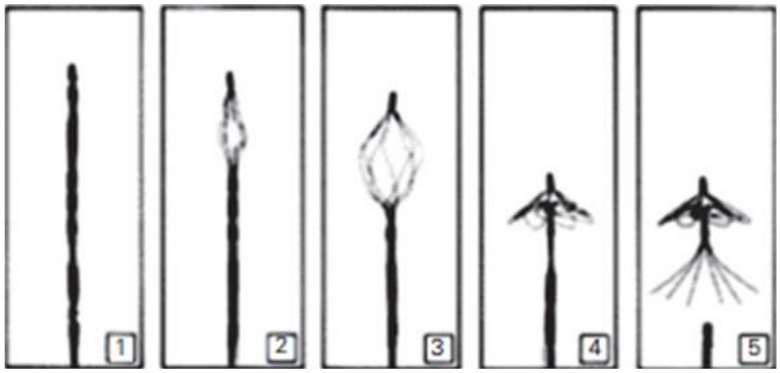

Figure 1.15: Sequence of deformed Simon filter attached to catheter [10]

Intravascular stent is by far the largest application of SMAs in medical field. A stent is a cylindrical structure that is used for cardiovascular applications to maintain the inner diameter of the blood vessel shown in Figure 1.16. This device uses the shape memory effect. Initially the material is in austenite phase, when cooled to M_f temperature the material is converted to twinned martensite phase [10]. The material is then deformed to detwinned state and placed

inside the blood vessel through catheter. Due to the body temperature, the stents recover its original shape [10].

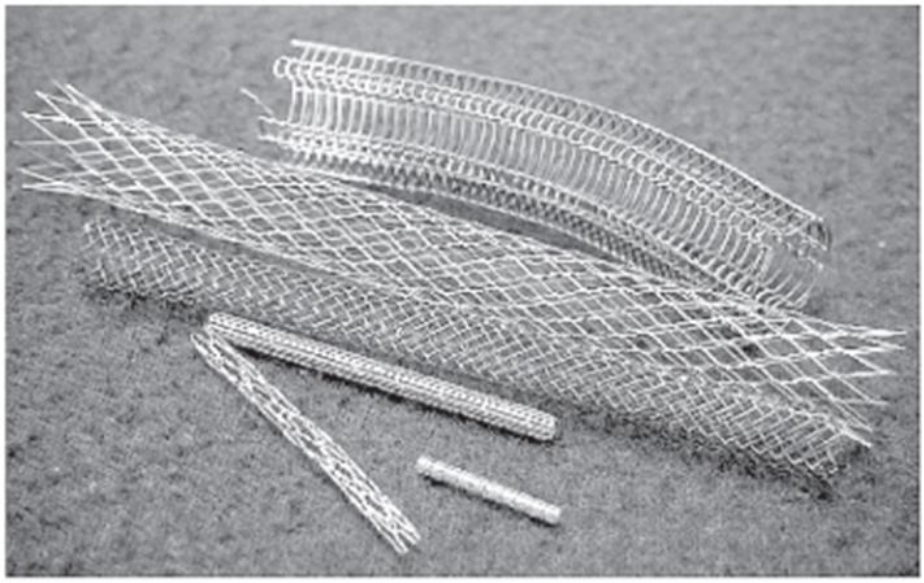

Figure 1.16: SMA stents [10]

In the orthopedic applications, SMAs are used in the form of vertebra spacer which is used to provide strength to the spinal vertebrae and to prevent motion during the healing process [9]. Theses spacers use the superelasticity phenomenon with the same principal used in dental bracers. Figure 1.17 shows shape memory spacer.

Figure 1.17: SMA vertebra spacer [9]

SMAs are also used to develop surgical instruments which are used to remove kidney, bladder and bile duct stones [1]. This instrument is initially in the shape of a basket; it is deformed and inserted into the human body. When the temperature reaches the austenite temperature, its shape recovery takes place [10]. It follows the same principal as the Simon filter; Figure1.18 shows the sequence of opening of the shape memory basket.

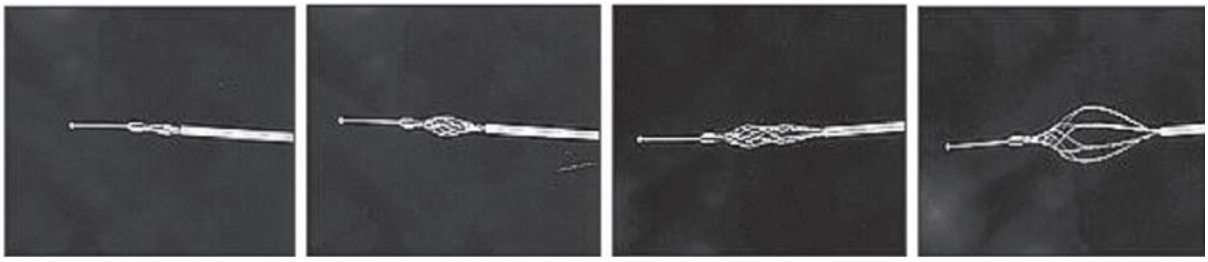

Figure 1.18: Sequence of opening of the shape memory basket [10]

1.6.3 Other Applications

SMA's are used in other fields such as automobiles, oil industries, rice cookers, civil structures, sporting goods and eye glasses. SMAs in these fields are used for the application of either impact absorption or actuation. The superelasiticity behavior is used by SMAs in armored vehicles in military, commercial applications and sporting goods to control impact absorption. It is also used to control the temperature of gearbox of Shinkansen bullet train [1]. SMA in the geometry of spring uses shape memory effect in this application. In order to control the temperature, the spring actuates a valve to adjust the oil level in the gearbox. The SMA in the form of valve is inserted in rice cooker, when the cooker reaches a certain temperature; it releases the excess steam in the chamber.

Figure 1.19: SMA actuators for damping [12]

To control the vibrations caused due to the earthquake, SMAs are used in civil structures [12] shown in Figure 1.19. The SMA actuators are in use for damping purposes, where each actuator is placed on the either side of the beam. When this beam bends in one direction, the bending mode is monitored. The sensor signal is sent to a micro-computer, where it is compared with a desired undisturbed position of the beam. The resulting signal helps Nitinol actuator on the other side to provide the control forces necessary to resist the beam vibrations.

1.7 Modeling of SMAs

Numerous research projects have focused on the area of constitutive modeling of SMAs over the past three decades. The majority number of the constitutive models in the literature is classified into either of the two groups:

i. Micromechanics models
ii. Phenomenological models

1.7.1 Micromechanics Model

By considering the behavior of a single grain of the alloy, this model predicts the response of the SMA. In the crystallographic modeling of a single grain, averaging the results over a

representative volume element to obtain a polycrystalline response of the SMA is the approach utilized by this type of model. This method of analysis for evaluating phase transformation in single crystals in SMA's has been presented by Patoor [13, 14]. The behavior of a polycrystalline SMA is modeled by utilizing the model for single crystals and using the self-consistent averaging method to account for the interactions between the grains.

A micromechanical model for SMAs are able to capture different effects of SMA behavior such as superelasticity, shape memory effect and rubber-like effect has been presented by [15]. In their work, the evolution of the martensitic volume fraction is obtained by balancing the internal dissipation during the phase transformation with the external energy output. One of the recent micromechanical models for SMA has been presented by [16]. The advantage of the crystallographical models is their ability to predict the material response using only the crystallographical parameters (e.g., crystal lattice parameters). Thus, their use provides valuable insight on the phase transformation process on the crystal level. However their disadvantage is that there is large number of numerical computations required to be performed which not feasible.

1.7.2 Phenomenological Model

In the case of phenomenological models, the change in material behavior due to phase transformation depends on the continuum thermo-mechanics of internal variables. These models usually assume a macroscopic energy function that depends on the internal variables used to describe the phase transformation. These models depend on a set of parameters extracted from experimental observations of SMA. E.g. modeling the shape memory effect response of SMA's in ANSYS. It involves different variables like hardening parameter, elastic limit, martensite modulus etc. which have to be determined by experimentation.

Some of the early 3-D models studied by using this type of analysis are Boyd and Lagoudas [17] and Tanaka [18]. In the studies done by Lagoudas [17] it has been shown that various phenomenological models can be unified under common thermodynamical formulation. In a recent work Qidwai and Lagoudas [19] presented a general thermodynamic framework for phenomenological SMA constitutive models, which for different choice of the transformation function can be tuned to capture different effects of the martensitic phase transformation, such as

pressure dependence and volumetric transformation strain. In addition to modeling of the development of transformation strain during martensitic phase transformation, several other modeling issues have also been topics of intensive research.

1.8 Fracture of SMAs

With the discovery of unique properties of SMA, its use in engineering and medical applications has increased. In parallel to this development, the number of studies investigating fracture properties of SMAs increased as well.

Yi and Gao [20] examined the fracture toughening mechanism of shape memory alloys under mixed mode loading at the martensite transformation. The studies show non-symmetric transformation boundaries for static and dynamic cracks. The results also showed that the reduction of crack tip energy release rate and increased toughness at the martensite transformation area. The studies by Auricchio [21] examined the martensitic transformations near the crack tip for a CT- specimen. The results showed that the size of the martensitic and transformation zones increases with the crack length. One of the earliest discussions on the effect of phase transformation on stress intensity factor (SIF) and toughness was studied by McMeeking and Evans [22]. The results show that the specimen undergoes stress-induced martensitic transformation and its toughness increases due to the residual strain field that restricts crack opening. Wang [23] investigated the effect of notch geometry on phase transformation and fracture toughness using compact tension (CT) specimens with different notch geometries under mode I loading. The results indicated that the amount of martensitic around the tip of a crack changes with the sharpness of the crack. The studies conducted by Baxevanis calculated the size and shape of the martensitic transformation region and J-integral near an edge-crack [24]. The studies by Birman [25] studied Mode I fracture using crack tip stress equations. The results show that the effect of phase transformation on the stress intensity factor is relatively small.

1.9 SMA based Actuators

SMAs with their unique thermo-mechanical properties are used as a potential material for actuators. The SMA uses the one-way shape memory effect to generate force and motion, which can be harnessed for actuator applications. SMA actuators can be used in various configurations including helical springs, cantilever strips, straight wires, torsion tubes and torsion springs [26].

The SMA actuators are not only used for motion generating applications but can also be used in advanced locking system. The specimen used in this work is a double notch specimen, which serves as a release mechanism for an enclosure. The enclosure is used in the application of deployment. The basic principle of this system is that, the SMA double notch specimen is constrained at one side and stretched over the gate to close it. In order to deploy, the SMA specimen should be fractured. In this work the SMA specimen is heated by passing electricity. When the temperature reaches austenite finish temperature the detwinned martensite crystals structure tries to convert to austenite structure. The crystal structure of austenite occupies less volume than the structure of martensite. Thus when material transforms to austenite the specimen tries to shrink, but since the specimen is constrained; high stresses are developed in the specimen. When the stress reaches the ultimate tensile stress the material fails.

For this to happen with higher accuracy, the material phases in the specimen have to be estimated since the mechanical properties of material phases are different.

The mechanical properties of SMAs are closely dependent on the temperature at which the mechanical properties are estimated. For example, SMAs exhibit the lowest yield strength at martensitic starting (M_s) temperature, and then the yield strength increases with increasing the temperature. This is because at this temperature the martensite structure can deform by moving twin boundaries which are quite mobile whereas in austenite the structure must deform by dislocation generation and movement. Thus the yield strength and the young's modulus of the martensite are extremely low compared to that of austenite.

Only certain amount of martensite deformation can be accommodated by this twin movement process and once the martensite is completely detwinned, the material will again deform elastically and eventually yield second time. Thus this ratio of resistance to reversible and irreversible deformation is thus characterized by the yield strength ratio of martensite to austenite. Table 1.1 highlights the young's modulus and yield strength of different SMAs.

With the addition of Cu to NiTi preferentially replaces Ni to form NiTiCu alloys. The addition of Cu reduces the hysteresis of the SMA response and also decreases the transformation strain there by decreasing the young's modulus when compared to NiTi alloy [1]. The addition of Cu also

reduces the sensitivity of the phase transformation temperatures. Due to the decrease in the hysteresis this alloy makes ideal choice for actuators.

Though NiTi SMAs offer excellent properties they are relatively expensive compared to the Copper based SMAs. Good electrical and thermal conductivity makes them attractive than NiTi alloy. The CuZn alloys are very ductile and have resistance to intergranular fracture compared to other Cu alloys. With the addition of Aluminum, the hysteresis

SMA	Material phase	Young's modulus (GPa)	Yield strength (MPa)
NiTi [28]	Martensite	28	70-140
	Austenite	87	200-700
NiTiCu [29]	Martensite	25	120
	Austenite	50	210
NiTiPd [29]	Martensite	15	100-150
	Austenite	25	200-240
CuAlNi [29]	Martensite	80	150-300
	Austenite	90	150-300
CuZnAl [30]	Martensite	70	80-300
	Austenite	70-100	150-350
49.2NiTi [31]	Martensite	35	60-120
	Austenite	68	180-600

Table 1.1: Young's modulus and yield strength of different SMAs.

curve increases, thus there is increase in the young's modulus. Cu-Al-Ni alloy is less sensitive to ageing. With varying the Al and Ni content the hysteresis and the phase transformation temperatures can be changed. The fracture toughness of martensite and austenite is shown in Table 1.2.

SMA	Material phase	Fracture Toughness ($MPam^{0.5}$)
52Ni48Ti [35]	Martensite	25
	Austenite	51.4
49.2NiTi [31]	Martensite	22.6
	Austenite	38.5

Table 1.2: Frature toughness of different SMAs.

1.10 Objective

The main objective of this work is to estimate the material phases in the SMA specimen which may be used in a release mechanism through a controlled failure. The specimen fails due to the high stresses produced during the phase transformation due to heating. Since the mechanical properties are different for austenite and martensite, the specimen behaves differently in different material phases. Thus in order to attain high accuracies with the controlled failure, the material phases has to be estimated in the specimen.

The second objective of this work is to study the behavior of the stress and material phases at different strain levels for different geometric configurations. The magnitude of the stress changes with different geometric configurations leading to different phase distributions. Such differences are expected to generate different failure paths.

1.11 Approach

To achieve the desired objectives a double notch specimen is modelled using a finite element analysis software tool ANSYS. A double notch configuration is selected in this work because

i. Since the present work deals with the controlled failure, the notches introduce stress concentration at defined locations.
ii. The equations describing the calculation of the stress concentration are readily available.

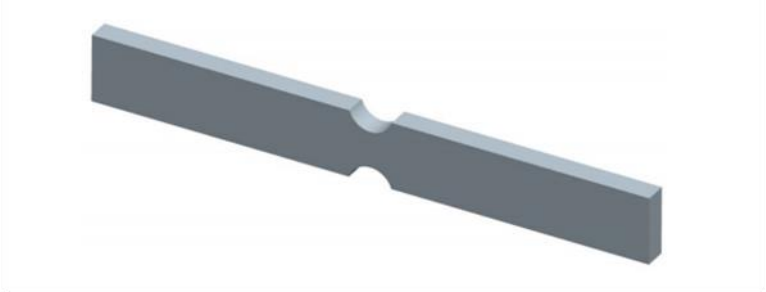

Figure 1.20: Double notch SMA specimen

Many applications involve devices made of SMAs, but the lack of efficient numerical tool hinders the development of such technologies. Software using FEA method like ANSYS allows the user to predict complex response. ANSYS describes the superelasticity and shape memory effect (SME) behavior of SMAs in detail. These behaviors are defined by a set of material parameters, which are estimated from the experimental data on NiTi alloy in the pseudoelastic phase and stress-temperature phase [27, 32, 33].

In this work the material phases are estimated by transformation strain tensor, which is not a standard output from ANSYS; it needs to be calculated based on strain results. This work, introduces a method of estimating the non-uniform distribution of material phases in SMAs at any given load by calculating the transformation strain in ANSYS. The transformation strain is estimated from the deviatoric strain tensors calculated at the end of load step. The deviatoric strains are calculated from the strain tensors. The mapping of phases that includes the mixed phases have not been done before. In the traditional format, the material phases are estimated from the stress-temperature plots shown in Figure 1.21. But, to construct this plot different parameters are required:

i. The initiation and completion temperatures for transformation from austenite to martensite at zero stress (M_s, M_f).
ii. The initiation and completion temperatures for transformation from martensite to austenite at zero stress ($A_s,\ A_f$).
iii. The stress influence coefficients or general slopes of the transformation surfaces. The zero-stress slopes of transformation regions into austenite given by C^A and into martensite given by C^M.

iv. The start and finish stresses for the detwinning of martensite (σ_s ,σ_f).

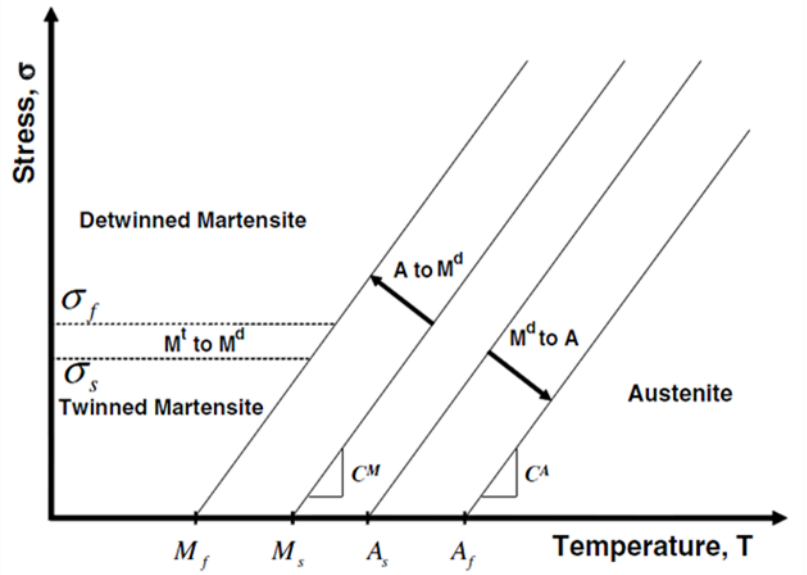

Figure 1.21 : Phase Transformation diagram [1]

These parameters can be either estimated from the experimental work or from different numerical tests in ANSYS. To estimate the zero-stress transformation temperatures, Differential scanning calorimetry (DSC) is used. The transformation temperatures at constant load are calculated from the isobaric testing. From these values the slopes of transformation regions can be constructed. The start and finish stresses for detwinning of martensite can be estimated from the loading and unloading test at temperature less than M_f.

But, this stress-temperature plot can be constructed for the problems involving traditional loading (loading- unloading). Since this work deals with a non-traditional loading path, the above stress- temperature plot cannot be constructed. Hence this work introduces a new approach for estimating the material phases in ANSYS.

Initially the specimen is at 225 ºK, so that the material is stable in twinned martensite phase. The specimen is subjected to two consecutive load steps. In the first load step, a tensile load is applied thereby changing the material phase to detwinned martensite. In the second load step by holding the specimen, it is uniformly heated to 1250 ºK. In this load step the material phase changes to austenite.

The transformation strain is estimated at the end of load step 1 and load step 2. The transformation contour plots are captured in ANSYS and the phase transformation is studied for different strain levels and for different geometric configurations.

CHAPTER 2 Thermo-mechanical Constitutive Modeling of Shape Memory Alloy

2.1 Introduction

This chapter introduces the three dimensional thermo-mechanical constitutive modeling of polycrystalline SMAs proposed by Souza et al. [27]. The main goal of this approach is to evaluate the different phases and as well as corresponding residual strain in the SMA. The phase transformations in SMAs due to application of stress or temperature are associated with dissipation of energy and the material is characterized by a highly nonlinear constitutive response. Due to higher stresses, the SMAs can be plastically deformed leading to complex description of the mechanical behavior. Hence, for the sake of simplicity the plastic deformations are not included in this work.

2.2 Constitutive Modelling

SMA's undergo phase transformation which is characterized by sequence of thermodynamic states that can be described by internal and external variables. In this model, the local thermodynamic state of the material is defined by the strain $\boldsymbol{\varepsilon}$ [27], which is given by;

$$\boldsymbol{\varepsilon} = \boldsymbol{\varepsilon}_e + \boldsymbol{\varepsilon}_T \tag{2.1}$$

In equation (2.1) $\boldsymbol{\varepsilon}_T$ denotes transformation strain which is defined as the strain developed due to phase transformation and $\boldsymbol{\varepsilon}_e$ denotes elastic strain.

The strain tensor, $\boldsymbol{\varepsilon}$ can be split into

$$\boldsymbol{\varepsilon} = \boldsymbol{e} + \frac{1}{3}(tr\ \boldsymbol{\varepsilon})\ I \tag{2.2}$$

In equation (2.2) $\boldsymbol{e}$ is the deviatoric strain, $(tr\ \boldsymbol{\varepsilon})$ is the volumetric strain and I is the identity tensor. The Cauchy stress tensor $\boldsymbol{T}$ is given by,

$$\boldsymbol{T} = \boldsymbol{S} + \frac{1}{3}(tr\ \boldsymbol{T})\ \ I \tag{2.3}$$

$$\boldsymbol{S} = \boldsymbol{T} - \boldsymbol{T}_m\, I \tag{2.4}$$

where, $\boldsymbol{S}$ is the deviatoric stress tensor and $\boldsymbol{T}_m$ is the mean stress.

Souza et al. [27] chose the strain $\boldsymbol{\varepsilon}$, volumetric component $tr\ \boldsymbol{\varepsilon}$ and deviatoric component $\boldsymbol{e}$, and the absolute temperature, θ, as control variables and a second-order tensor, transformation strain, $\boldsymbol{\varepsilon}_T$ as internal variable. The transformation strain $\boldsymbol{\varepsilon}_T$ is equal to its deviatoric part $\boldsymbol{e}_T$. The basic principal of this model is, when the material is in its parent phase i.e. austenite or twinned martensite, the transformation strain is equal to 0, shown in equation (2.5).

$$\left|\left|\boldsymbol{e}_T\right|\right| = 0, \tag{2.5}$$

If the material is in its product phase, detwinned martensite phase, the value of transformation strain is ξ_s.

$$\left|\left|\boldsymbol{e}_T\right|\right| = \xi_s \tag{2.6}$$

If value of the transformation strain is between 0 and ξ_s, the material phase is the mixture of austenite and detwinned martensite or twinned martensite and detwinned martensite.

$$0 < \left|\left|\boldsymbol{e}_T\right|\right| < \xi_s, \tag{2.7}$$

The variable ξ_s in equation (2.7) is defined as the amount of strain associated with the detwinned martensitic variant. From considering the above variables and from the conservation laws, the Helmholtz free energy function (ψ) is written as [1]:

$$\psi(tr\boldsymbol{\varepsilon}, \boldsymbol{e},\ \boldsymbol{e}_T, \theta) = \left(\frac{\lambda}{2} + \frac{\mu}{3}\right)(tr\ \boldsymbol{\varepsilon})^2 + \mu\left|\left|\boldsymbol{e} - \boldsymbol{e}_T\right|\right|^2 + \tau_M(\theta)\ \left|\left|\ \boldsymbol{e}_T\right|\right| + \frac{h}{2}\ \left|\left|\boldsymbol{e}_T\right|\right|^2 + I_{\xi_s}(\boldsymbol{e}_T) \tag{2.8}$$

In equation (2.8) the variables λ, μ are the Lamé constants of the material, h is a material parameter related to hardening of the material during phase transformation and $\tau_M(\theta)$ is a positive function of the temperature θ and $I_{\xi_s}(\boldsymbol{e}_T)$ is the indicator function associated with transformation strain defined as;

$$I_{\xi_s}(\boldsymbol{e}_T) = \begin{cases} 0 & \text{if } \left|\left|\ \boldsymbol{e}_T\right|\right| \leq 0 \\ +\infty & \text{otherwise} \end{cases} \tag{2.9}$$

In order to enforce inequality constraint (equation (2.7)), the thermodynamic equilibrium state of material point is expressed in terms of quantities thermodynamically conjugate to the $tr\ \boldsymbol{\varepsilon}, \boldsymbol{e},\ \boldsymbol{e}_T$ and $\boldsymbol{\theta}$. By definition:

$$\boldsymbol{T}_m = \left(\lambda + \frac{2\mu}{3}\right) tr\ \boldsymbol{\varepsilon} \tag{2.10}$$

$$\boldsymbol{S} = 2\ \mu\ (\boldsymbol{e} - \boldsymbol{e}_T) \tag{2.11}$$

$$\boldsymbol{X} = \boldsymbol{S} - (\tau_M(\theta)\partial\left|\left|\ \boldsymbol{e}_T\right|\right| + h\ \boldsymbol{e}_T + \partial I_{\xi_s}(\boldsymbol{e}_T)) \tag{2.12}$$

with $\boldsymbol{X}$ indicated in the following as transformation stress, In the phase transformation process ($0 < \left|\left|\boldsymbol{e}_T\right|\right| < \xi_s$), $\boldsymbol{X}$ is given by

$$\boldsymbol{X} = \boldsymbol{S} - \left(\tau_M(\theta) + h\left|\left|\,\boldsymbol{e}_T\right|\right| + \gamma\right)\frac{\boldsymbol{e}_T}{\left|\left|\boldsymbol{e}_T\right|\right|} \tag{2.13}$$

The variable γ results from the indicator function sub-differential $\partial I_{\xi_s}(\boldsymbol{e}_T)$ and is defined as

$$\begin{cases} \gamma = 0 \text{ if } 0 < \left|\left|\,\boldsymbol{e}_T\right|\right| < \xi_s \\ \gamma \geq 0 \text{ if } \quad \left|\left|\,\boldsymbol{e}_T\right|\right| = \xi_s \end{cases} \tag{2.14}$$

The variable $\boldsymbol{X}$ in equation (2.13) is the driving force for the phase transformation processes and we can interpret it as back stress which defines the origin of the elastic domain. The mechanical dissipation inequality reduces to

$$D^{mech} = \boldsymbol{X}\!:\dot{\boldsymbol{e}}_T \geq 0 \tag{2.15}$$

where, the dissipation is defined as the rate of internal entropy production per unit volume times the absolute temperature. It is also defined as the Clausius–Duhem inequality. To satisfy the second law of thermodynamics or the mechanical dissipation inequality (equation (2.15)), we choose the following flow rule for the internal variable:

$$\dot{\boldsymbol{e}}_T = \dot{\zeta}\,\frac{\boldsymbol{X}}{\left|\left|\boldsymbol{X}\right|\right|} \tag{2.16}$$

To describe phase transformation evolution, a function *f* defined as:

$$f = \left|\left|\boldsymbol{X}\right|\right| - R \tag{2.17}$$

where, the material parameter R is the elastic region radius. The model is finally completed by describing the criteria for elastic behavior and phase transformation.

i. For elastic behavior:

$$\dot{\boldsymbol{e}}_T = 0 \tag{2.18}$$

$$\boldsymbol{e}_T = 0 \quad \text{and} \quad \left|\left|\boldsymbol{S}\right|\right| < \tau_M(\boldsymbol{\theta}) + R \tag{2.19}$$

ii. In phase transformation:

$$\dot{\boldsymbol{e}}_T = \dot{\zeta}\,\frac{\boldsymbol{X}}{\left|\left|\boldsymbol{X}\right|\right|} \quad \text{and} \quad \dot{\zeta} > 0 \tag{2.20}$$

$$0 < \left|\left|\,\boldsymbol{e}_T\right|\right| < \xi_s\,,\ X = \boldsymbol{S} - \left(\tau_M(\theta) + h\left|\left|\,\boldsymbol{e}_T\right|\right|\right)\frac{\boldsymbol{e}_T}{\left|\left|\boldsymbol{e}_T\right|\right|} \text{ and } \left|\left|\boldsymbol{X}\right|\right| = R \tag{2.21}$$

iii. Saturated phase transformation:

$$\dot{\boldsymbol{e}}_T = \dot{\zeta}\,\frac{\boldsymbol{X}}{\left|\left|\boldsymbol{X}\right|\right|} \quad \text{and} \quad \dot{\zeta} > 0 \tag{2.22}$$

$$\left|\left|\,\boldsymbol{e}_T\right|\right| = \xi_s\,,\ \boldsymbol{X} = \boldsymbol{S} - \left(\tau_M(\theta) + h\left|\left|\,\boldsymbol{e}_T\right|\right| + \gamma\right)\frac{\boldsymbol{e}_T}{\left|\left|\boldsymbol{e}_T\right|\right|} \text{ and } \left|\left|\boldsymbol{X}\right|\right| = R \tag{2.23}$$

Figure 2.1 describes the phase transformation when load is applied. The horizontal region abcd, depicts the parent phase which is either martensite or austenite. Phase transformations take place only along the line cf and the surface cdef shows the mixtures of phases. A saturated phase transformation is represented by horizontal region efgh.

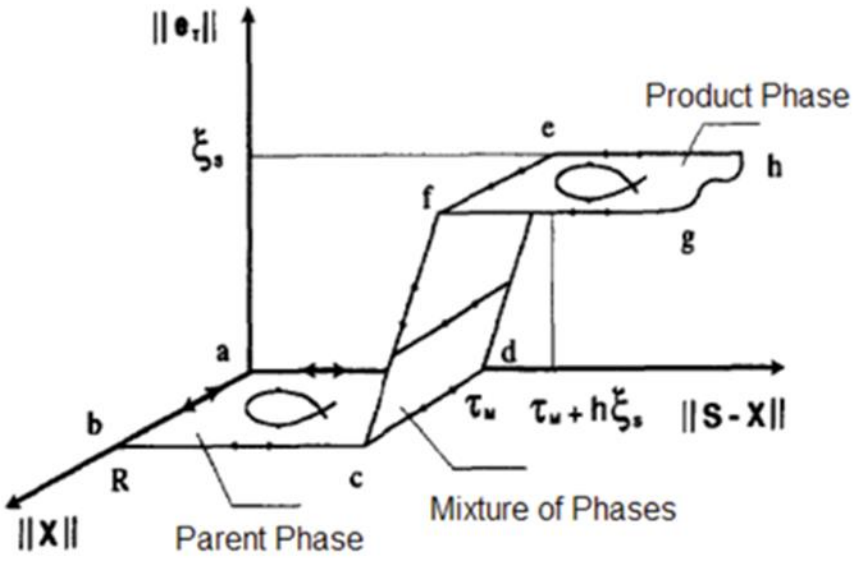

Figure 2.1: Relevant paths for phase transformation [27]

CHAPTER 3 Finite Element Modeling of Thermo-mechanical Element

3.1 Introduction

This chapter focuses on the finite element modelling of the SMA material geometry and also describes the procedure involved to calculate the phase transformation.

The finite element analysis (FEA) method is a powerful computational approach used to solve real world engineering problems. It solves by creating subdivisions of a whole problem domain into simpler parts, called finite elements. Different methods such as variational calculus or weighted residuals method are utilized. To obtain solution to engineering problems by using FEA, one needs a computer program which is based on FEA formulation or commercial software like ANSYS or ABAQUS. In the present work, ANSYS 14.5 software is used. ANSYS is a multi-purpose analysis tool that can be used in various engineering disciplines. The engineering simulation product provides a complete set of element behavior, material models and equation solvers for a wide range of mechanical design problems.

As discussed in previous chapters, to observe the phase transformation in the SMA, it is either subjected to stress or temperature. In this work, to estimate the phase transformation, the SMA specimen is initially mechanically loaded, and then heated to elevated temperature. At this high temperature, the austenite and martensite phases are identified in the specimen.

3.2 Geometry Description

ANSYS theory manual describes the superelasticity and shape memory effect (SME) behavior of SMAs in detail. These behaviors are defined by a set of material parameters, which are estimated from the experimental data on NiTi alloy in the pseudoelastic phase and stress-temperature phase [27,32,33]. Souza in his paper [27] explained about the work done by Sittner on Cu-Al-Zn-Mn polycrystalline SMA. From the experimental and numerical work on Cu-Al-Zn-Mn

polycrystalline SMA a set of material parameters are derived. Table 3.1 shows the material parameters used.

Constant	Meaning	Value
C1	h (Mpa)	9230
C2	T_o (K)	253.15
C3	R (Mpa)	73.4
C4	β (Mpa)	4.2
C5	ε_L	0.1
C6	E_m (Mpa)	30.7X 10^3
C7	m	0

Table 3.1 : Material parameters of Cu-Al-Zn-Mn polycrystalline SMA [27]

The constants in Table 3.1 represent,

C1- Hardening parameter

C2- Reference temperature

C3- Elastic limit

C4- Temperature scaling parameter

C5- Maximum transformation strain

C6- Martensite modulus

C7- Symmetric behavior

The double notch specimen geometry considered in this work is shown in Figure 3.1. The geometry is a 2-D specimen with length 70 mm and width 6 mm. The notches have radius of 2 mm. The specimen is analyzed by assuming plane strain conditions. The other conditions in the plane strain are:

$$\varepsilon_Z = \gamma_{XZ} = \gamma_{YZ} = 0 \tag{3.1}$$

and

$$\tau_{XZ} = \tau_{YZ} \tag{3.2}$$

For meshing purpose, 2-D Plane 182 quadrilateral elements are used. These elements are defined by four nodes having two degrees of freedom at each node.

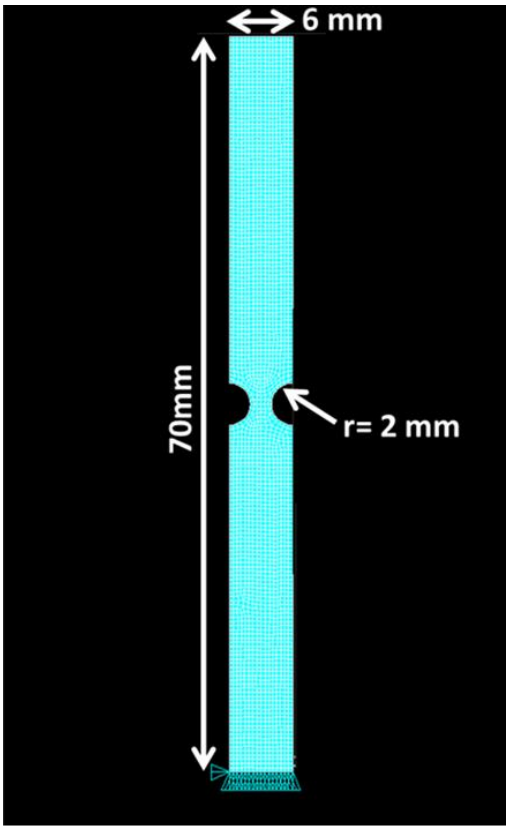

Figure 3.1: 2-D double notch geometry

3.2.1 Boundary Conditions

In this problem, the conditions along the boundary are defined as follows

$$U_x\ (x=0,y=0) = 0;\ U_y\ (x=0,\ y=0) = 0;\ \text{and} \tag{3.3}$$

$$U_y\ (x,y=0) = 0 \tag{3.4}$$

which means, at the origin (x,y) =(0,0) the specimen is fixed. The bottom surface of the specimen (y=0) cannot move in y-direction, as shown in Figure 3.1. Before the material parameters are used for this specimen for analysis, they should be validated. The next section explains about the validation and its results.

3.3 Verification Problem

Prior to simulating the double notch specimen behavior under the two load steps described earlier, a verification problem is considered to ensure the correct usage of ANSYS material model. For this purpose, the problem considered by Sittner et al [34] is chosen. The specimen is a 120 mm long tube with inner diameter of 12 mm. Since the cross-section and loading are identical on planes passing through the longitudinal central axis, axisymmetric 2-D elements are used in ANSYS. Figure 3.2 shows the ANSYS model.

The 2-D plane-183 type elements with element size of 1.2 mm are used for the meshing purpose. With the assumed element size, the total numbers of elements formed in the specimen are 280. The boundary conditions used for this analysis are;

$$Ux\ (x=0,y=0) = 0\ ;\ Uy\ (x=0,y=0) = 0 \tag{3.5}$$

$$Uy\ (x,y=0) = 0 \tag{3.6}$$

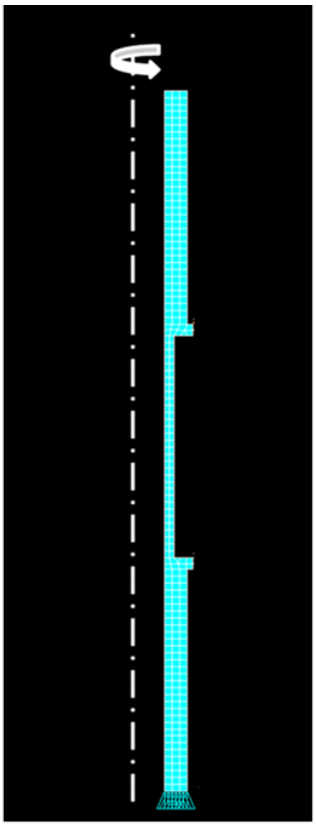

Figure 3.2: 2-D Tensile specimen with axisymmetric behavior

In ANSYS, the specimen is loaded in two load steps. In load step 1, the specimen is loaded axially in + y-direction by applying displacement of 1.48 mm. The displacement is applied at the top surface (y=120) of the specimen. In load step 2, the specimen is unloaded to the initial position. The results from ANSYS include stress and strain calculated at the center of gauge length. A stress-strain plot is calculated and verified with the stress-strain plot from the results of Sittner [34] as shown in Figure 3.3.

In the verification process, the strain values of both the results are compared at four different stress-strain values. These values are the points on the plot where the phase transformations take place. When the results are compared with the results from Sittner et al [34], it is calculated that the results from ANSYS differ by from 1.1 %- 1.8% shown in Table 3.2.

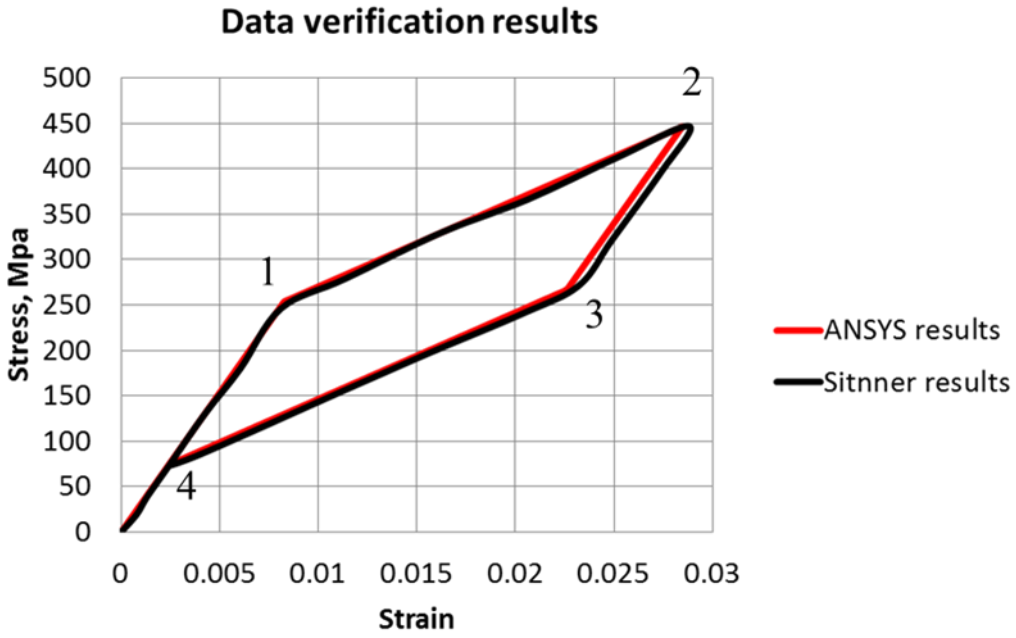

Figure 3.3: Stress-strain behavior calculated by ANSYS compared to Sitnner et al [34].

S.No	ANSYS results	Sitnner results	Difference (%)
1	0.00816	0.00801	1.8
2	0.0283	0.0288	1.73
3	0.0228	0.02322	1.84
4	0.00251	0.00248	1.19

Table 3.2 : Verification of Sitnner and ANSYS results

3.4 Mesh Density

In order to establish that the mesh refinement level is sufficient for acceptable accuracy, a total of three mesh refinement levels were analyzed. For case 1, element size of 1.2 mm is used. For cases 2 and 3, element sizes 0.9 mm and 0.6 mm are used, respectively. The loading and boundary conditions are identical to the verification problem. Figure 3.4 shows the stress-strain results from different mesh sizes. The stress-strain data are in close agreement across the refinement levels. It is concluded that the mesh size of 1.2 mm is sufficient for this study.

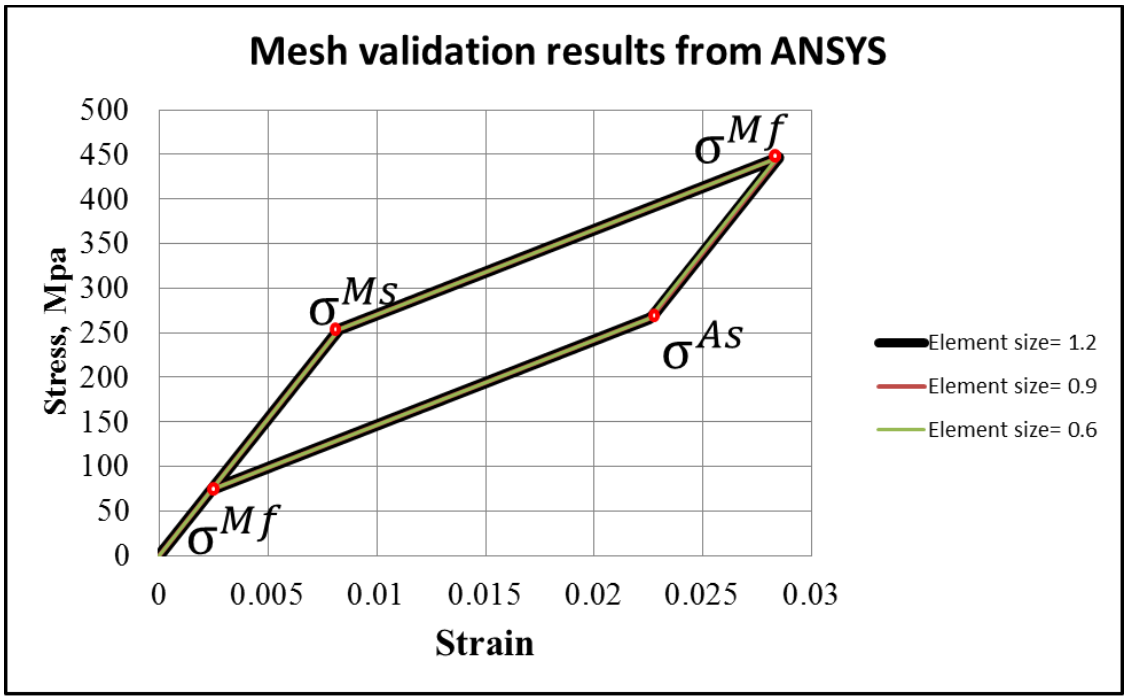

Figure 3.4: Mesh validation results

3.5 Loading Conditions on Double Notch Specimen Simulations

Since, the properties are validated; the next step is to construct a process to observe the phase transformation in ANSYS. The initial temperature of the specimen is 253.15 $^{\circ}$K, the specimen is cooled to 225 $^{\circ}$K to obtain a stable martensite phase. In this work, to observe the phase transformation two load steps used.

In load step 1, a mechanical loading is applied in tensile direction on the top surface of the specimen. In the load step 2, while holding the specimen under tension, a uniform temperature increase of 225 $^{\circ}$K to 1250 $^{\circ}$K is applied. The code used for this problem is included in Appendix A.

Three different strain loading cases are studied for this geometry. In case 1, a strain of 6.5% is applied in load-step 1. In case 2, 8.5% strain is applied and in case 3 10.7% strain is applied and in the load step 2, while holding the specimen under tension, the temperature is increased from 225 $^{\circ}$K to 1250 $^{\circ}$K. The output results are in the form of 1st principal stress maps and transformation strain maps of the specimen at the end of each load step for different geometric configurations, which will be discussed in the next chapter.

3.6 Calculation of Transformation Strain

The transformation strain ($||e_T||$) is calculated from the equation (3.7) as the difference between the modulus of deviatoric total strain ($||e_{tot}||$) and the deviatoric elastic strain ($||\boldsymbol{e}_{el}||$).

$$||\boldsymbol{e}_T|| = ||\boldsymbol{e}_{tot}|| - ||\boldsymbol{e}_{el}|| \tag{3.7}$$

The deviatoric total strain tensor e_{tot} is given by:

$$\boldsymbol{e}_{tot} = \boldsymbol{\varepsilon}_{tot} - \frac{1}{2}\,(tr\,\boldsymbol{\varepsilon}_{tot})\,I \tag{3.8}$$

where, $\boldsymbol{\varepsilon}_{tot}$ is the total strain generated in the specimen at the end of load-step. It is represented by,

$$\boldsymbol{\varepsilon}_{tot} = \begin{bmatrix} \boldsymbol{\varepsilon}_{11} & \boldsymbol{\varepsilon}_{12} \\ \boldsymbol{\varepsilon}_{21} & \boldsymbol{\varepsilon}_{22} \end{bmatrix} \tag{3.9}$$

where, $\boldsymbol{\varepsilon}_{11}$ is the total strain generated in x-direction, $\boldsymbol{\varepsilon}_{22}$ is the total strain generated in y-direction and $\boldsymbol{\varepsilon}_{12}$ is the total shear strain in xy direction. Since, $\boldsymbol{\varepsilon}_{12} = \boldsymbol{\varepsilon}_{21}$ and $\boldsymbol{\varepsilon}_{tot}$ is given by,

$$\boldsymbol{\varepsilon}_{tot} = \begin{bmatrix} \boldsymbol{\varepsilon}_{11} & \boldsymbol{\varepsilon}_{12} \\ \boldsymbol{\varepsilon}_{12} & \boldsymbol{\varepsilon}_{22} \end{bmatrix} \tag{3.10}$$

From equation (3.8), (3.9) and (3.10) the deviatoric total strain is given by;

$$\boldsymbol{e}_{tot} = \begin{bmatrix} \boldsymbol{e}_{11} & \boldsymbol{e}_{12} \\ \boldsymbol{e}_{12} & \boldsymbol{e}_{22} \end{bmatrix}$$

where, $\boldsymbol{e}_{11}$ is the deviatoric strain in x-direction $\boldsymbol{e}_{22}$ is the deviatoric strain in y-direction and $\boldsymbol{e}_{12}$ is the deviatoric shear strain. $\left|\left|\boldsymbol{e}_{tot}\right|\right|$ is represented by,

$$\left|\left|\boldsymbol{e}_{tot}\right|\right| = \sqrt{\boldsymbol{e}_{11}^2 + \boldsymbol{e}_{22}^2 + 2\boldsymbol{e}_{12}^2} \tag{3.11}$$

With the same procedure, using same equation for elastic strains $\left|\left|\boldsymbol{e}_{el}\right|\right|$ is calculated;

$$\left|\left|\boldsymbol{e}_{el}\right|\right| = \sqrt{\boldsymbol{e}_{11el}^2 + \boldsymbol{e}_{22el}^2 + 2\boldsymbol{e}_{12el}^2} \tag{3.12}$$

Where $\boldsymbol{e}_{11el}, \boldsymbol{e}_{22el}, \boldsymbol{e}_{12el}$ are the deviatoric elastic strains in x, y and xy directions. The $\left|\left|\boldsymbol{e}_{tot}\right|\right|$ and $\left|\left|\boldsymbol{e}_{el}\right|\right|$ from equation (3.11) and (3.12), respectively, are used to calculate the transformation strain $\left|\left|\boldsymbol{e}_{T}\right|\right|$ using equation (3.7).

CHAPTER 4 Results

4.1 Introduction

This chapter describes the results obtained from ANSYS, the results are in form of transformation strain, 1st principal and 2nd principal stress contour plots. The results are obtained for three different applied strain level's 6.5%, 8.5%, and 10.7% at the end of load step 1 and load step 2 for different geometric configurations.

4.2 Results

In this work, five different geometric configurations are studied. The specimen with the two notches at the center of the specimen is considered as the base specimen. The specimen for which the notches are shifted vertically by 5 mm from the center of the specimen in +y and –y direction is labelled as A1 specimen. The specimen for which the notches are shifted vertically by 10 mm from the center of the specimen in +y and –y direction is labeled as specimen A2. Figure 4.1 shows the graphical comparison of base, A1 and A2 specimens.

The other two cases considered in this work are, B1 (for which the center of the notch is shifted by r/3 mm in x and –x directions) and B2 (for which the center of the notch is shifted by distance 2 r/3 mm in x and –x directions). These specimens are labeled as B1 and B2 specimens. In Figure 4.2, graphical depictions of the base, B1 and B2 specimens are given.

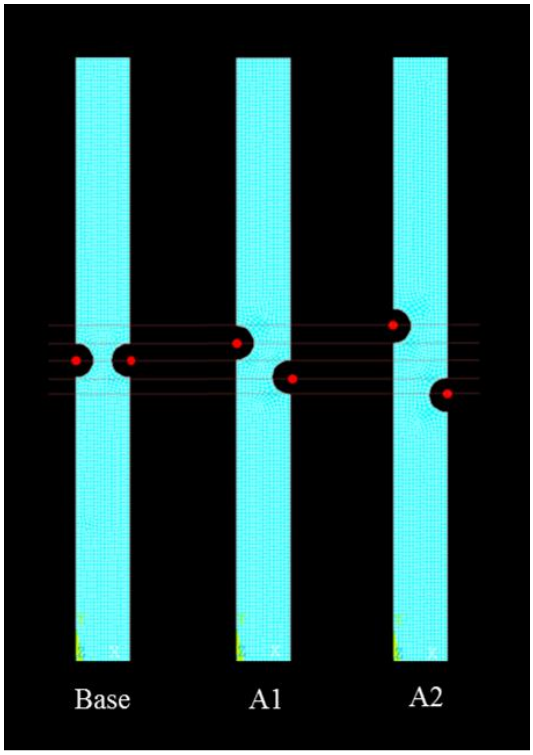

Figure 4.1: Comparison of base, A1 and A2 specimens

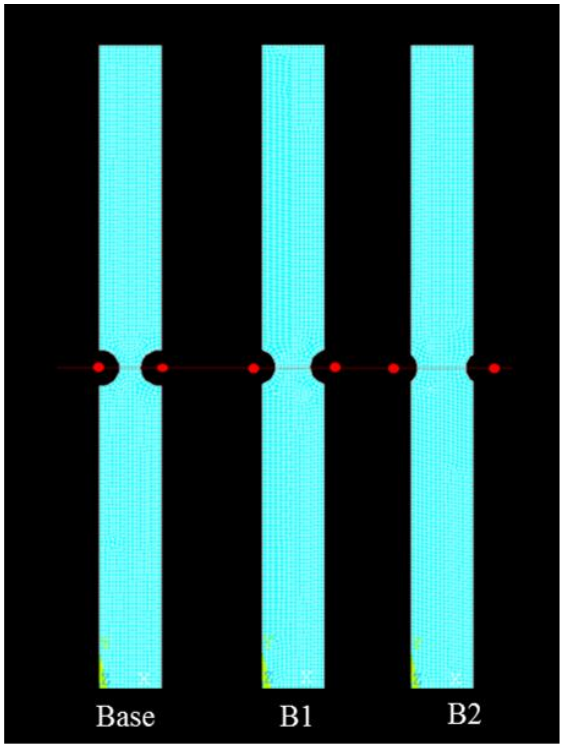

Figure 4.2: Comparison of base, B1 and B2 specimens

Three distinct load levels are applied in each specimen: 6.5%, 8.5%, and 10.7% strain in y-direction. Table 4.1 provides a complete list of the cases considered along with the case numbers assigned.

Case number	Geometric configurations	Strain levels(%)
1	Base	6.5
2	Base	8.5
3	Base	10.7
4	A1	6.5
5	A1	8.5
6	A1	10.7
7	A2	6.5
8	A2	8.5
9	A2	10.7
10	B1	6.5
11	B1	8.5
12	B1	10.7
13	B2	6.5
14	B2	8.5
15	B2	10.7

Table 4.1: List of cases considered

Figure 4.3 presents the contour plots of transformation strain for the first geometry variation (A1,A2) as well as the base specimen for loading levels 6.5%, 8.5%, and 10.7% strain at the end of load step 1. In all the specimens, if the transformation strain is 0, the material at that region is considered to be in twinned martensite phase. If the transformation strain is equal to the maximum value of transformation strain than the material phase is considered to be pure detwinned martensite. If the value of transformation strain is between zero and the maximum value of transformation strain than, the material is considered to be mixture of twinned and detwinned martensite.

In all the cases, it is observed that as the strain levels in the specimen increases, the transformation strain increases. From the Figure 4.3, it is observed that the transformation strain is maximum at a point on the notch which is away from stress concentration point. This is because at these points the shear strain is maximum and the transformation strain is related to deviatoric components.

In case 1, the transformation strain is maximum between the notches and as the notches are shifted vertically (cases 4 and 7) the transformation strain path changes. When compared with the A2 specimens, the transformation strain is maximum for A1 specimens. This is due to the geometry; the notches are close to each other for A1 specimens.

While holding the specimen in tension the specimen is heated uniformly in the load step 2. The transformation strain contour plots at the end of load step 2 for different displacements are shown in Figure 4.4. From the literature it is learnt that when the material is in detwinned martensite phase and is heated, at a certain temperature the material transforms to austenite phase. By the same principle, in this work when the specimen is heated, the material transforms to austenite phase. At higher temperatures the austenite phase is stable, hence it is considered to be as the parent phase. At higher loads and higher stresses the material phase transforms to detwinned martensite phase thus it is considered to be product phase. Hence when compared with the literature the results can be quantified as, if the magnitude of transformation strain is 0 the material is in austenite phase. If magnitude of transformation strain is maximum, then the phase is in detwinned martensite phase. If the value of transformation strain is between 0 and the maximum transformation strain, the material is considered to be mixture of twinned martensite, detwinned martensite and austenite. It is observed that the magnitude of transformation strain decreases in load step 2. This is the indication that the material phase is transforming to austenite phase.

From the Figure 4.4, it can also be interpreted that with the notched closer to each other a detwinned martensite phase path can be observed between the notches. With the eccentricity of the notches the detwinned material path decreases. Hence we can state that with the shifting in the notches, the material phases can be changed.

Figure 4.5 presents the contour plots of 1st principal stresses for base, A1 and A2 specimens at end of load step 1. The maximum 1st principal stress is 7311.75 MPa and it is observed at the stress concentration area for case 9. It is observed that, as the displacement is increased, the principal stress at the notches increases. The 1st principal stresses are maximum as the eccentricity of the specimen increases. The principal stresses are related to the shear stress and the other combined stresses in the specimen.

In the load step 2, it is observed that the value of maximum principal stress 14335.1 MPa. It is almost double the value of principal stress in load step 1. This is because, when the specimen is heated the material transforms to austenite. The crystal structure of austenite is cubic structure lattice, which occupies less volume than the orthorhombic crystal structure of detwinned martensite. In austenite phase the specimen tries to shrink. But, since the specimen is constrained, it is not able to shrink. Due to this high stress is generated in the specimen; which can be explained in Figure 4.6.

Thus in real time application, when the specimen is constrained and stretched the SMA specimen transforms to detwinned martensite phase. At this point when the SMA specimen is heated to high temperature, the SMA specimen breaks thus, allowing the material to deploy.

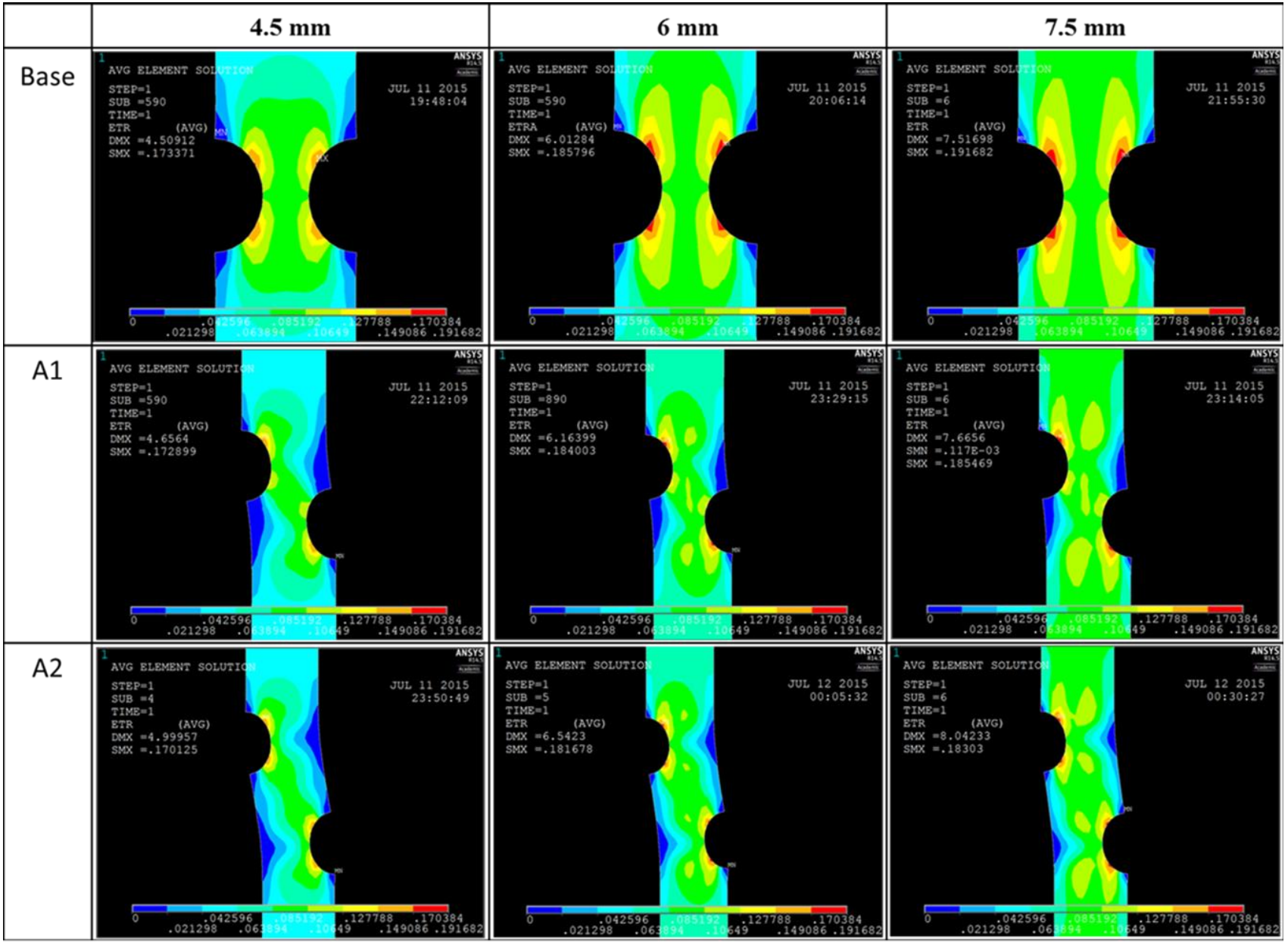

Figure 4.3 : Contour plots of transformation strain for base, A1, A2 at the end of load step 1

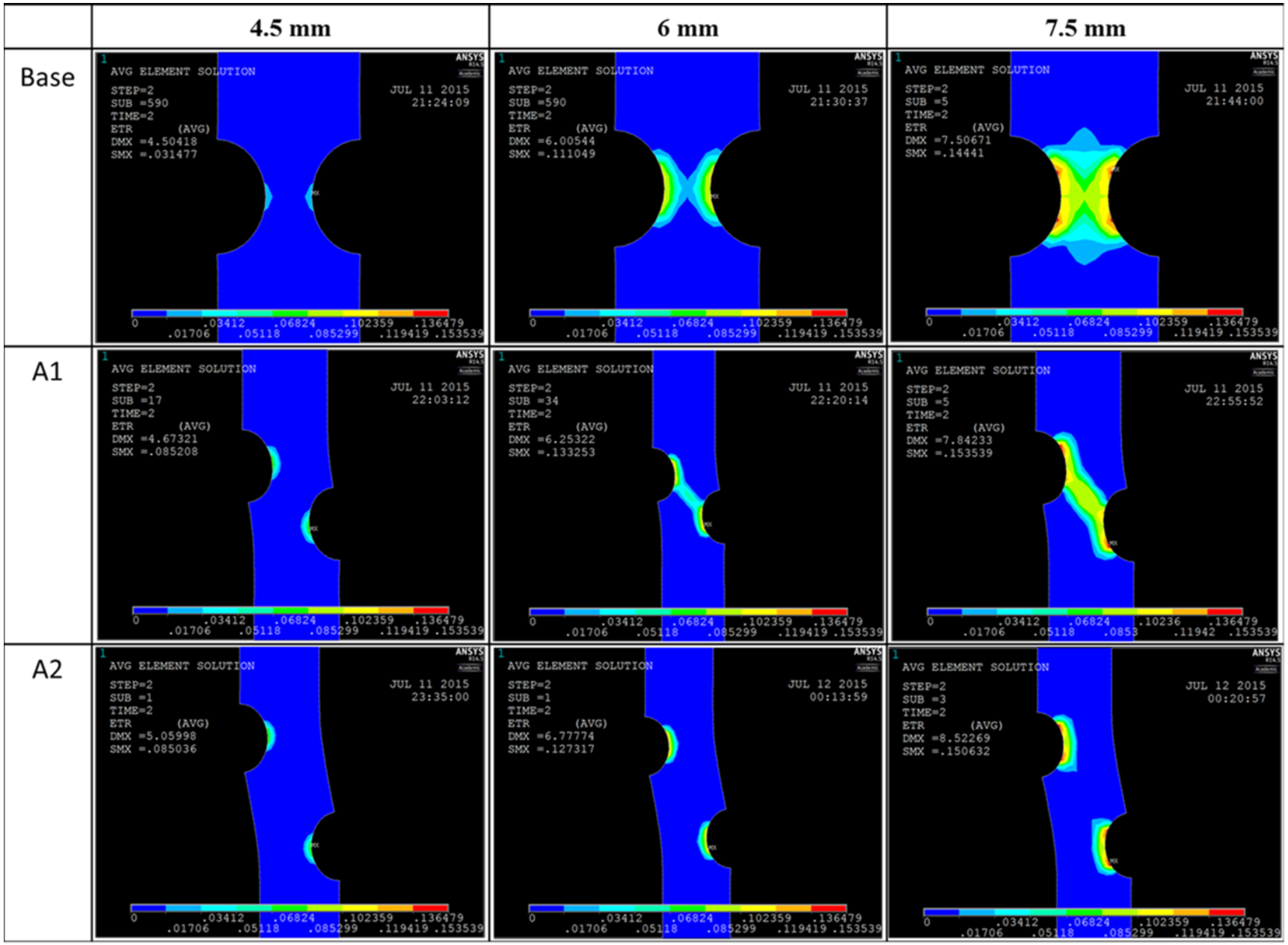

Figure 4.4 : Contour plots of transformation strain for base, A1, A2 at the end of load step 2

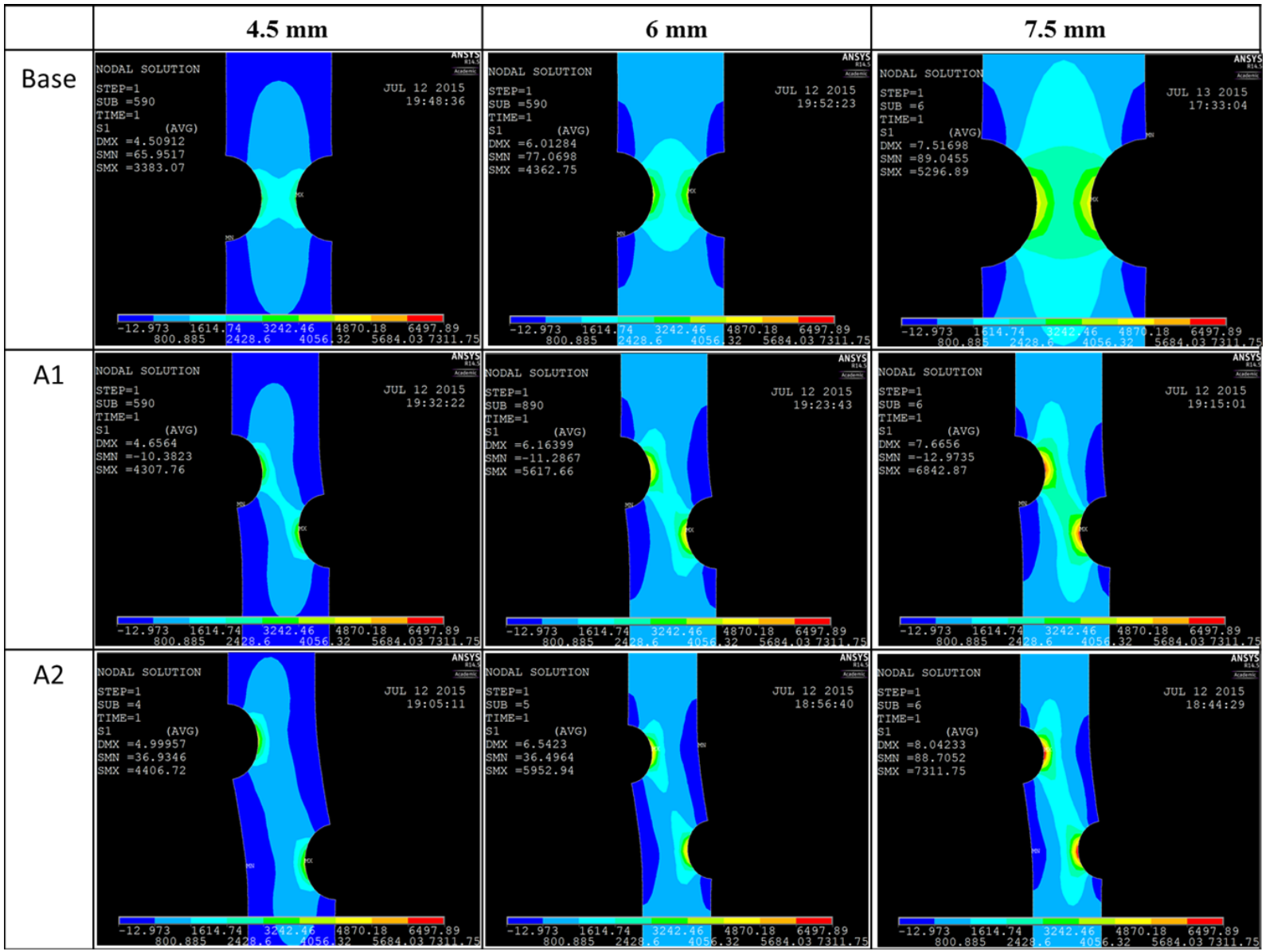

Figure 4.5: Contour plots of 1st principal stress for base A1, and A2 specimens at load step 1

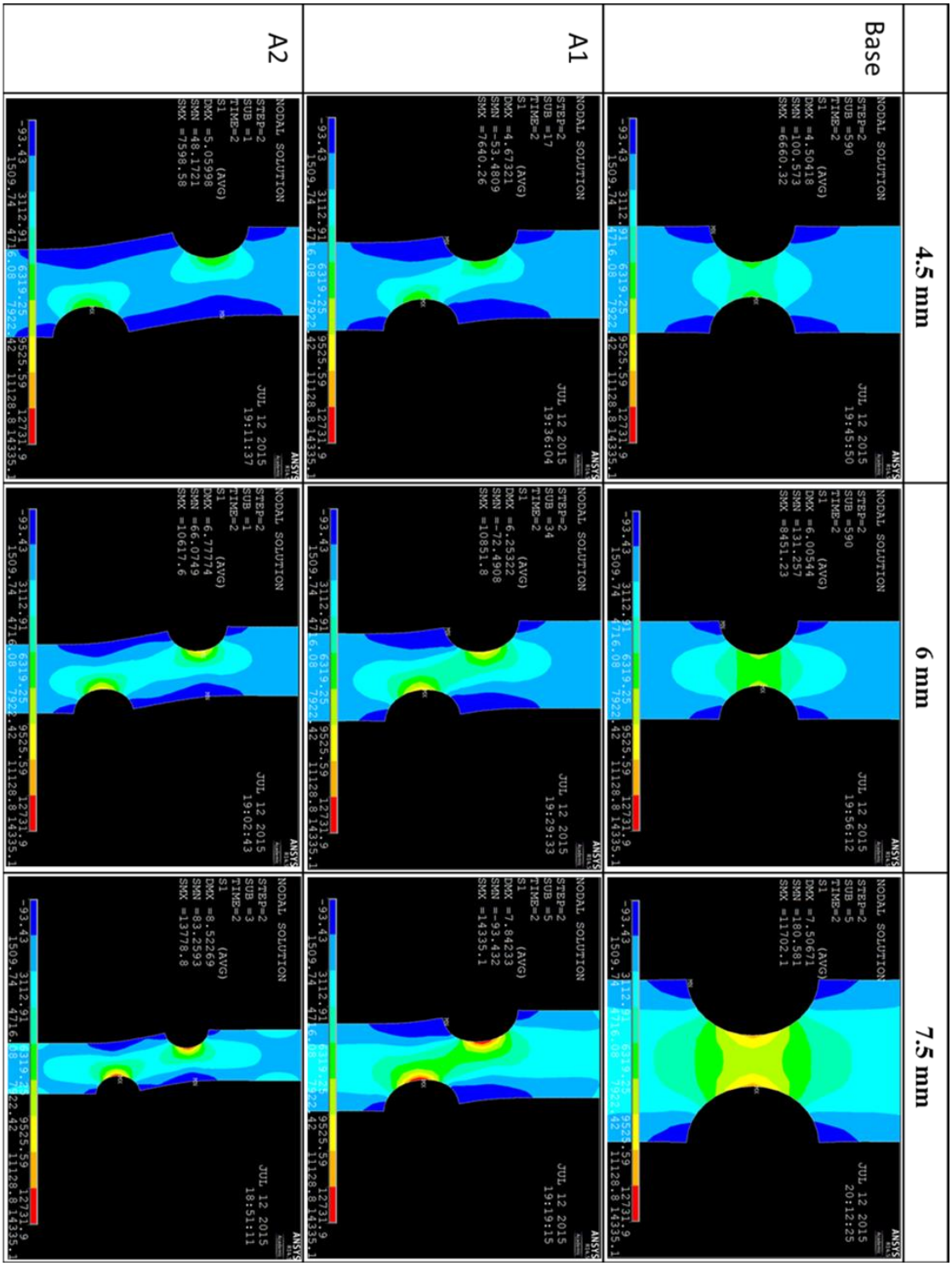

Figure 4.6 : Contour plots of 1st principal stess for base, A1, A2 at the end of load step 2

In addition to the contour plots, the principal stress, principal strains and temperature are analyzed as a function of load at three different points. Figure 4.7 shows three different points considered for the base specimen. The principal stresses and strains are plotted for 6.5%, 8.5%, and 10.7% strains.

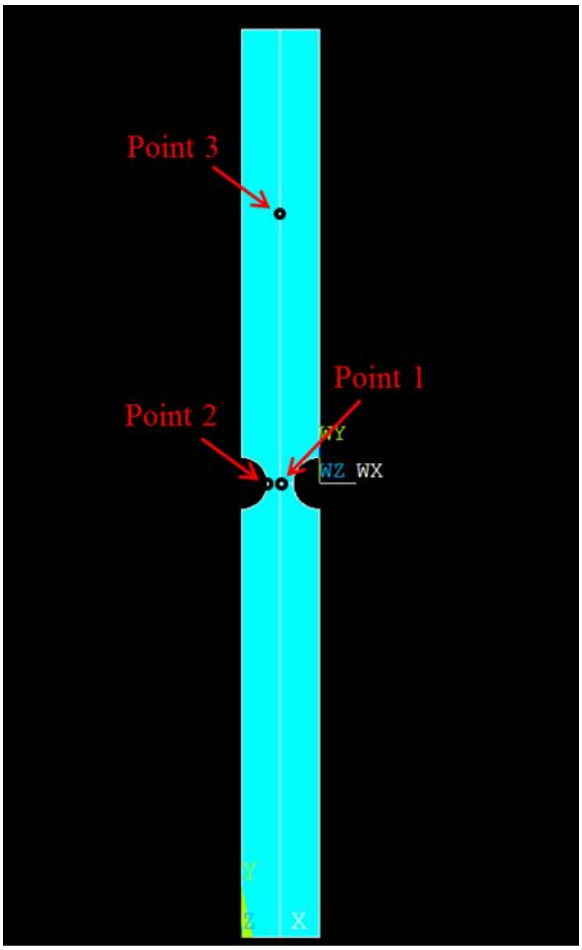

Figure 4.7: Stress, Strain located at specific points

From these plots, a complete trace of twinned and detwinned martensite can be indicated. Figure 4.8 represents the principal stress, principal strain and temperature plot at point 1 for 10.7 % strain. The boxed numbers in Figure 4.8 and subsequent similar figures indicate the sub-step number out of the 640 total sub-steps. The top right figure is the 3-D plot and the other plots are the 2-D plots of same plot. From the 3-D plot in Figure.4.8 it can be depicted that at sub-step 2 the detwinning of the specimen starts. At sub-step 233 the material converts completely into the detwinned phase. The end of load step 1 is marked by the sub-step 320. At this stage the specimen is heated uniformly to 1250 ºK. At 280 ºK (at sub-step 340) the stress starts increasing linearly. This is because initially the material is in martensite phase at sub-step 340, the material at this points starts converting to austenite.

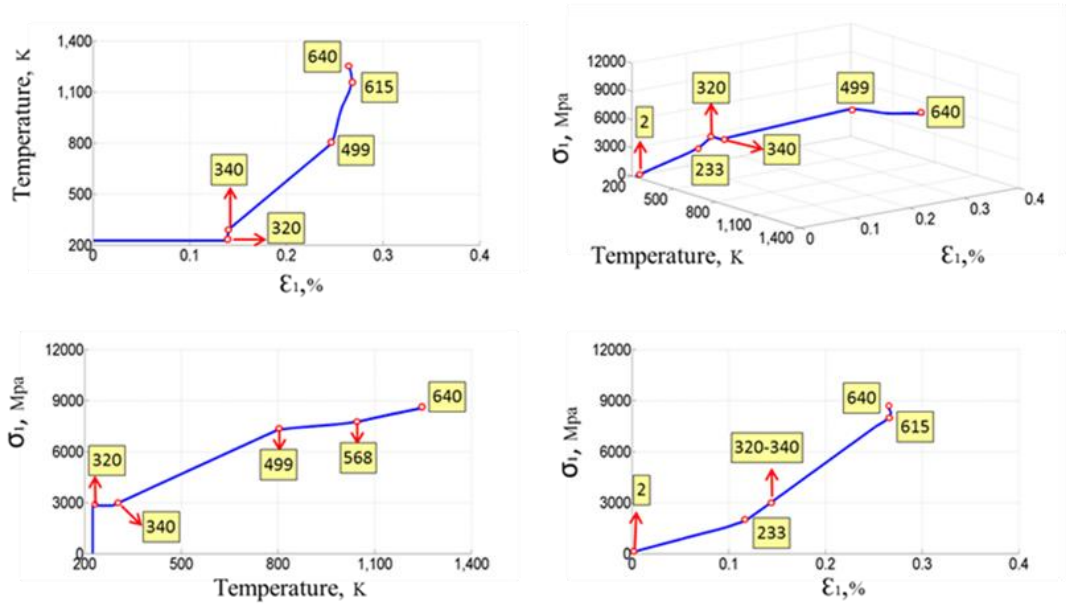

Figure 4.8: Principal stress, principal strain at point 1 for 10.7% strain

When further heated, at sub-step 499 the stress and temperature increases but the strain becomes almost constant. This is because at this sub-step the material starts to transform to complete austenite, but since the material is constrained the material phase remains in detwinned martensite. When further heated at sub-step 615 the stress increases but the strain decreases slightly until sub-step 640. This is because of the austenite phase present, hence we can't find the maximum transformation at this point from the transformation strain maps.

Figure 4.9 presents the principal stress, principal strain and temperature behavior at point 2. Since this point is a stress concentration point the material at this points detwinns earlier than point 1. From the Figure 4.9 it can be observed that the material starts detwinning at sub-step 109 which is earlier than point 1. The material phase at this point is pure detwinned martensite at the end of load step-1 at sub-step 320. In load step 2, the specimen is heated to 1250 ºK. At the sub-step 340 when the temperature reaches 280 ºK, the stress increases linearly up to sub-step 499. This is because at this temperature the material hits austenite start temperature and the austenite phase transformation starts. With the further increase in the temperature at sub-step 581, the material converts to austenite. This process can be justified with the decrease in the strain up to sub-step 640.

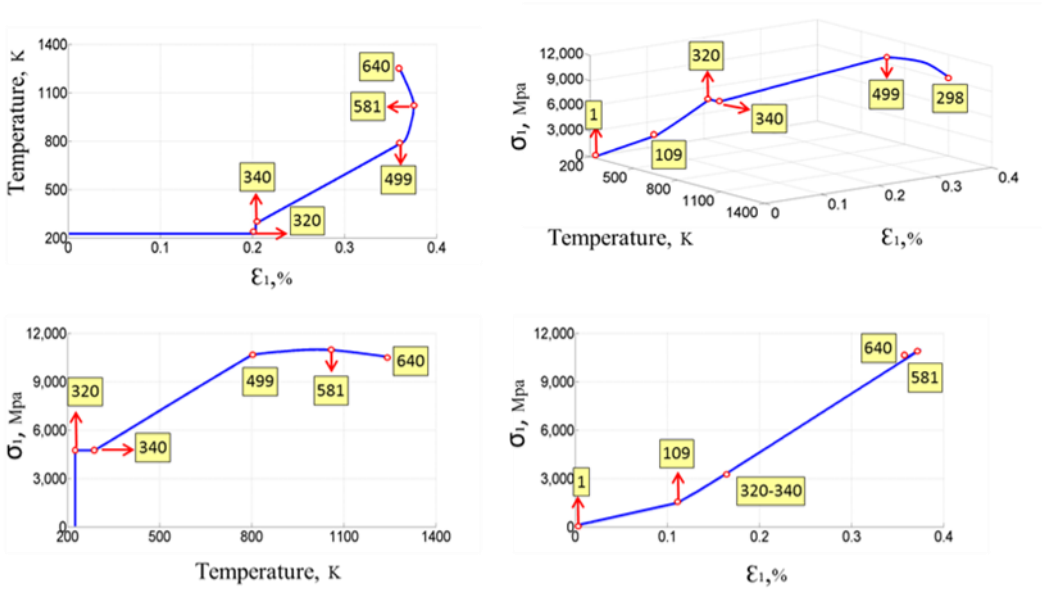

Figure 4.9: Principal stress, principal strain at point 2 for 10.7% strain

Figures 4.10 presents the 3-D and 2-D plots of principal stress, principal strain and temperature at point 3. Since this point is away from the stress concentration region, the stress at this point is less compared to other two points. From the Figure 4.12, we can interpret that in load step 1 the materials starts to detwinn at sub-step 4. When further loaded the material phase remains mixture of twinned and detwinned martensite at the end of load step 1. In load step 2 when the material is heated to 1250 ºK at sub-step 340 the material reached austenite start temperature. At this phase the material is mixture of austenite, twinned and detwinned martensite. In this stage the material at this point shrinks. This is because the material at point 1 and 2 expands and since all the points are in same continuum, the strain at point 3 decreases. With further increase in the temperature at sub-step 500 the material transforms to complete austenite.

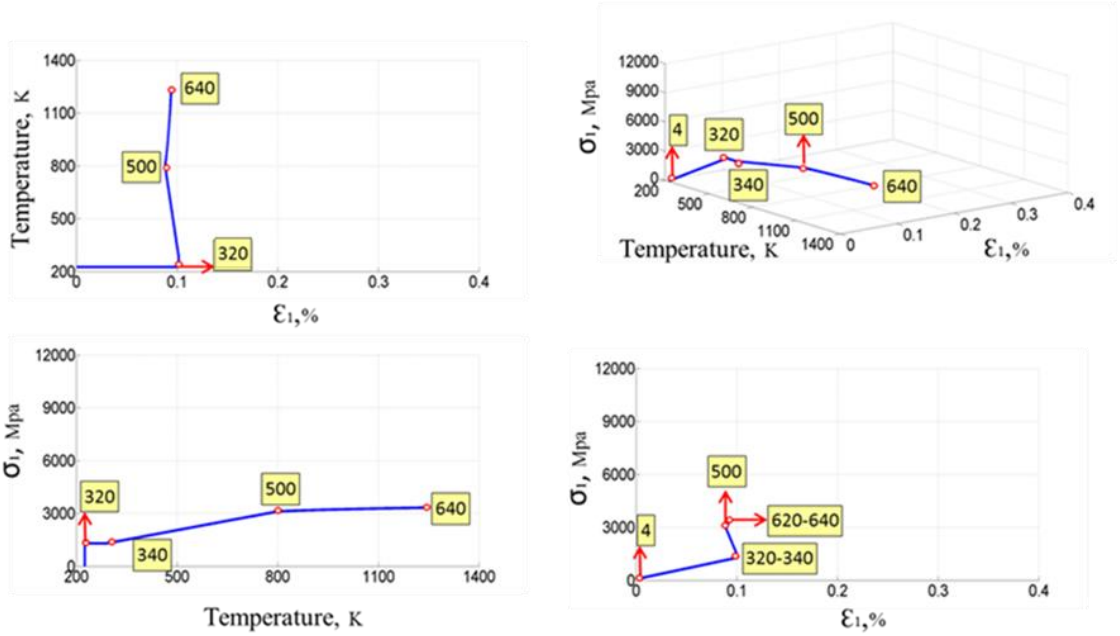

Figure 4.10: Principal stress, principal strain at point 3 for 10.7% strain

From the results pertaining to Figures 4.8 through 4.10 it is interpreted that, the material phases at point 1 (sub-step 109) transformed into complete detwinned martensite, when the material phases at other points are still a mixture of twinned and detwinned martensite. This is because this point is the stress concentration point and has maximum stress thus the material detwinns at early stage. The material phase at point 2 has reached complete detwinned martensite phase at sub-step 233. Since point 2 is away from the stress concentration point, the material detwins at a later stage. We can also see that point 3 is still in mixture of twinned and detwinned martensite mixture when point 1 and 2 are completely detwinned martensite. The results can also be quantified with the Figure 4.11 where a plot between transformation strain and the number of sub-steps is plotted. From Figure 4.11 it can be interpreted that Point 2 has detwinned early compared with point 1 and point 3. At the end of load step 2 it can be seen that the material at point 2 is mixture of twinned and detwinned martensite, point 3 is in complete austenite phase and the material at point 1 is the mixture of martenite and austenite. These results can also be validated with the transformation strain contour maps for 10.7% strain.

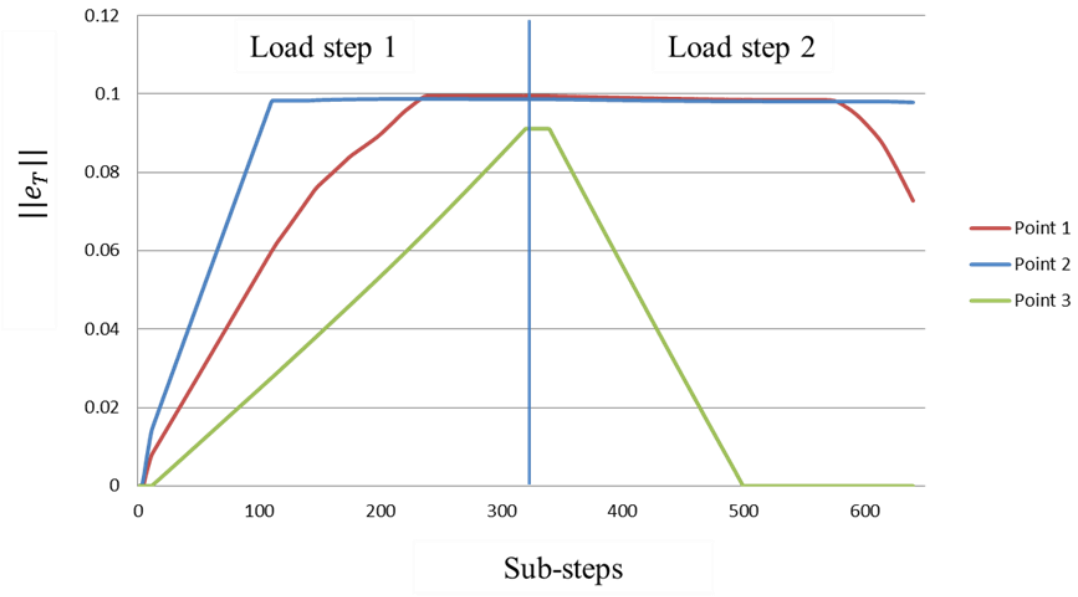

Figure 4.11: Transformation vs sub-steps

Figure 4.12 represents the principal stress, principal strain and temperature data at point 1 for 8.5% strain. From the 3-D plots we can depict that, in load step 1, when the material is axially loaded the material reaches detwinning start stress at sub-step 6. When it is further loaded the principal stress reaches detwinning finish stress at sub-step 298 where the material phase transforms to complete detwinned martensite. At sub- step 320 load step 2 starts, where the specimen is heated to 1250K. When the temperature reaches 280 K at sub-step 340, the principal stress increases linearly till the sub-step 466. This is due to the same reason discussed for 10.7% strain data. At sub-step 541 with further increase in the temperature the stress increases with the decrease in the principal strain. At this sub-step the material transforms into austenite.

The principal stress, principal strain and temperature 3-D plot at point 2 for 8.5% strain is given in Figure 4.13. From the above figure we can depict that, when the material is axially loaded the material reaches detwinning start stress at sub-step 4. When it is further loaded the principal stress reaches detwinning finish stress at sub-step 138 where, the material phase transforms to

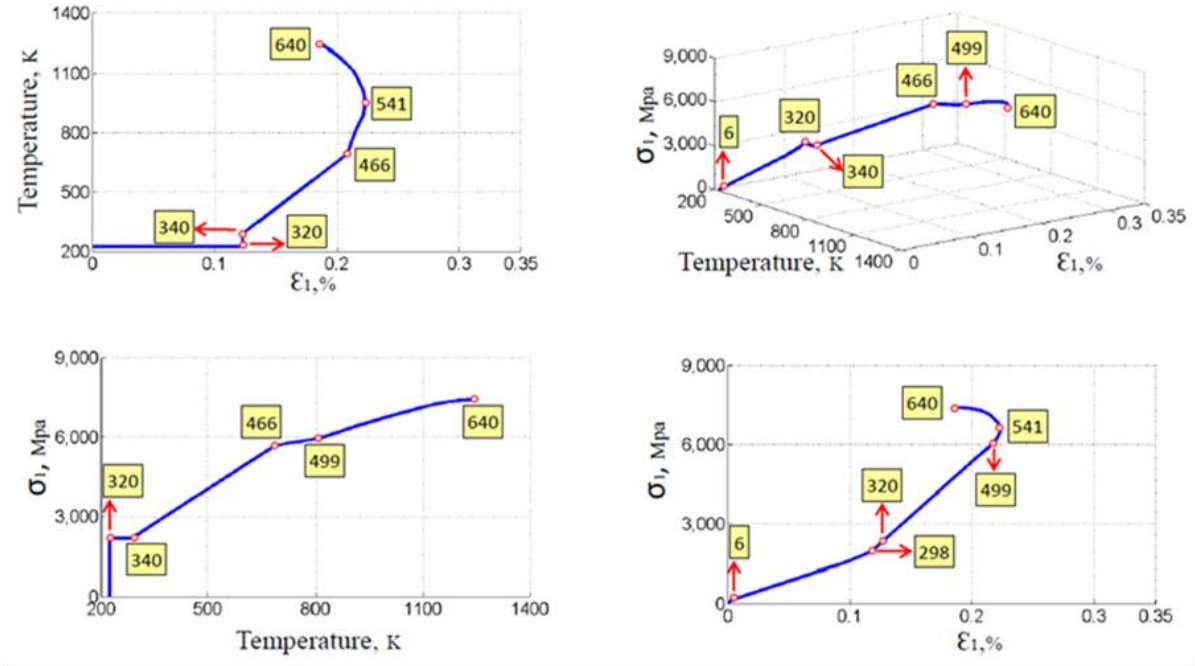

Figure 4.12: Principal stress, principal strain at point 1 for 8.5% strain

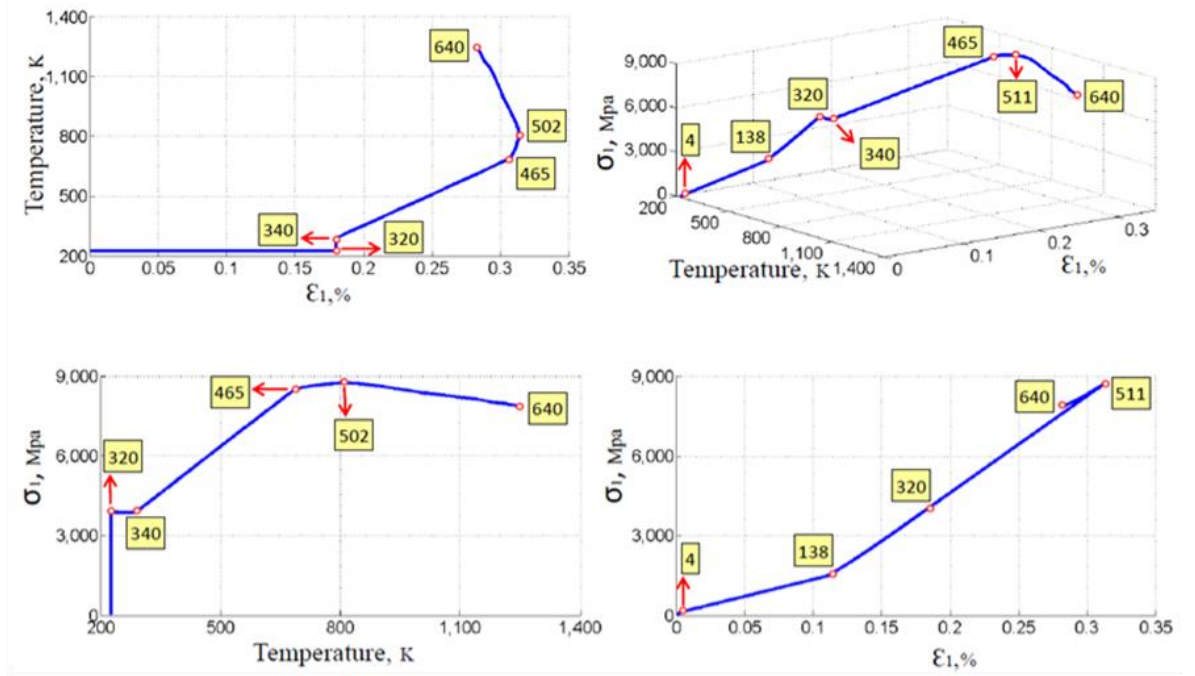

Figure 4.13: Principal stress, principal strain at point 2 for 8.5% strain

complete detwinning martensite. At sub- step 320, load step 2 starts, where the specimen is heated to 1250K. When the temperature reaches 280 K at sub-step 340, the stress increases linearly till the sub-step 502 due to the same reason that the material transforms to austenite phase. At this sub-step with further increase in the temperature the stress increases with the decrease in the principal strain.

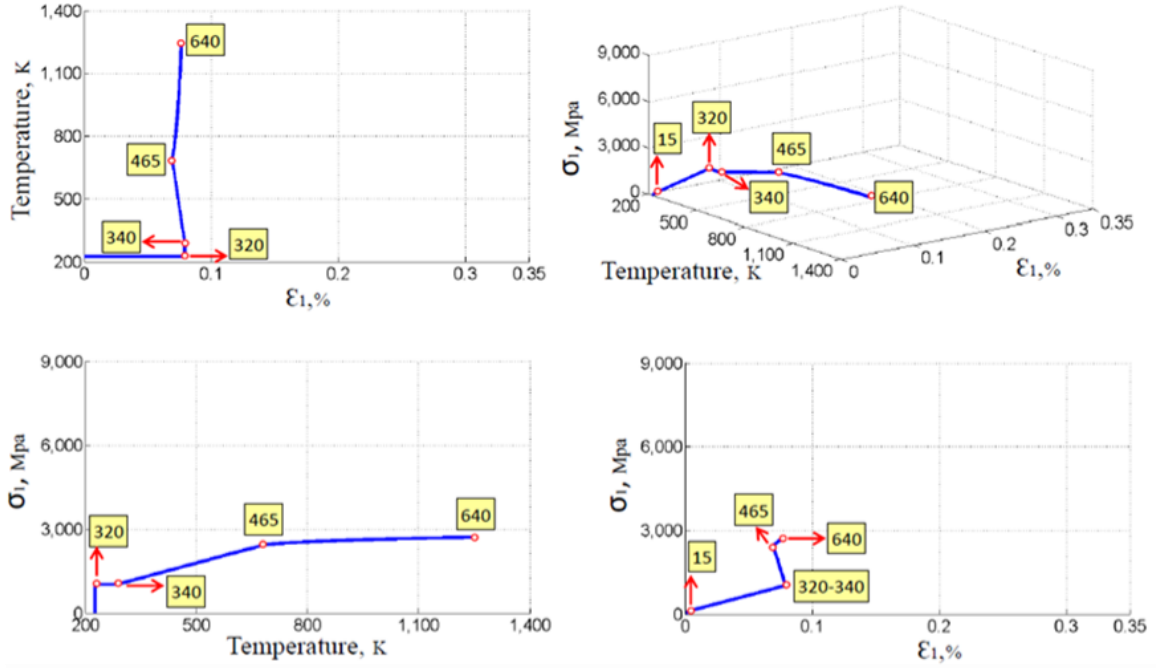

Figure 4.14: Principal stress, principal strain at point 3 for 8.5% strain

Figures 4.14 presents the 3-d and 2-d plots of principal stress, principal strain and temperature at point 3. Since this point is away from the stress concentration region, the stress at this point is less compared to other two points. From the Figure 4.14, we can interpret that in load step 1 the materials starts to detwinn at sub-step 15. When further loaded the material phase remains mixture of twinned and detwinned martensite at the end of load step 1. In load step 2 when the material is heated to 1250K at sub-step 340 the material reached austenite start temperature. At this phase the material is mixture of austenite, twinned and detwinned martensite. In this stage the material at this point shrinks. This is because the material at point 1 and 2 expands and since all the points are in same continuum, the strain at point 3 decreases. With further increase in the temperature at sub-step 500 the material transforms to complete austenite.

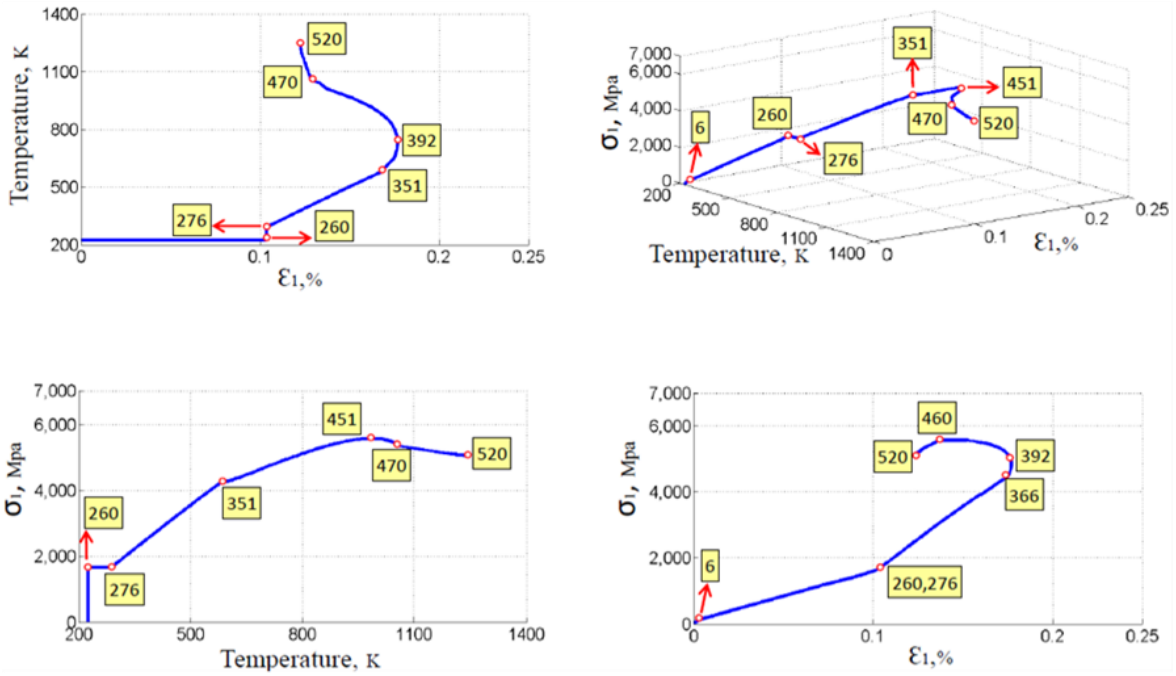

Figure 4.15: Principal stress, principal strain at point 1 for 6.5% strain

Figure 4.15-4.17 shows the principal stress, principal strain and temperature 3-D plot at points 1,2 and 3 for 6.5% strain. In order to converge the solution a total of 520 sub-steps are used. In load step 1, it can be observed that the material at point 1 detwins at sub-step 6 and material at point 2 at sub-step 4 respectively. At point 2 the material transforms to complete detwinned martensite at sub-step 150. The material phase at point 3 is in mixture of twinned and detwinned martensite at end of load step 1. The material is uniformly heated to 1250 ºK during load step 2. When the temperature reaches 280 ºK at sub-step 276 the stress increases and strain increases at point 1 and point 2 but the strain decreases at point 3. With further increase in the temperature the stress increases and strain decreases. At points 3 and 4 with the increase in temperature, the stress increases and the strain decrease is very slightly.

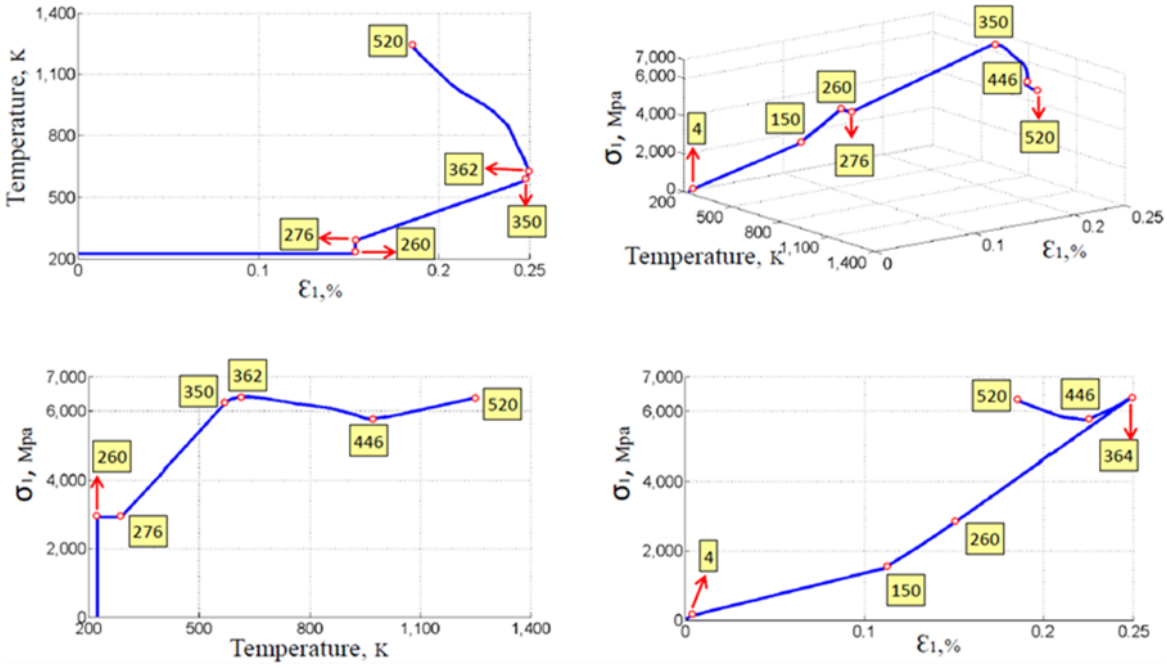

Figure 4.16: Principal stress, principal strain at point 2 for 6.5% strain

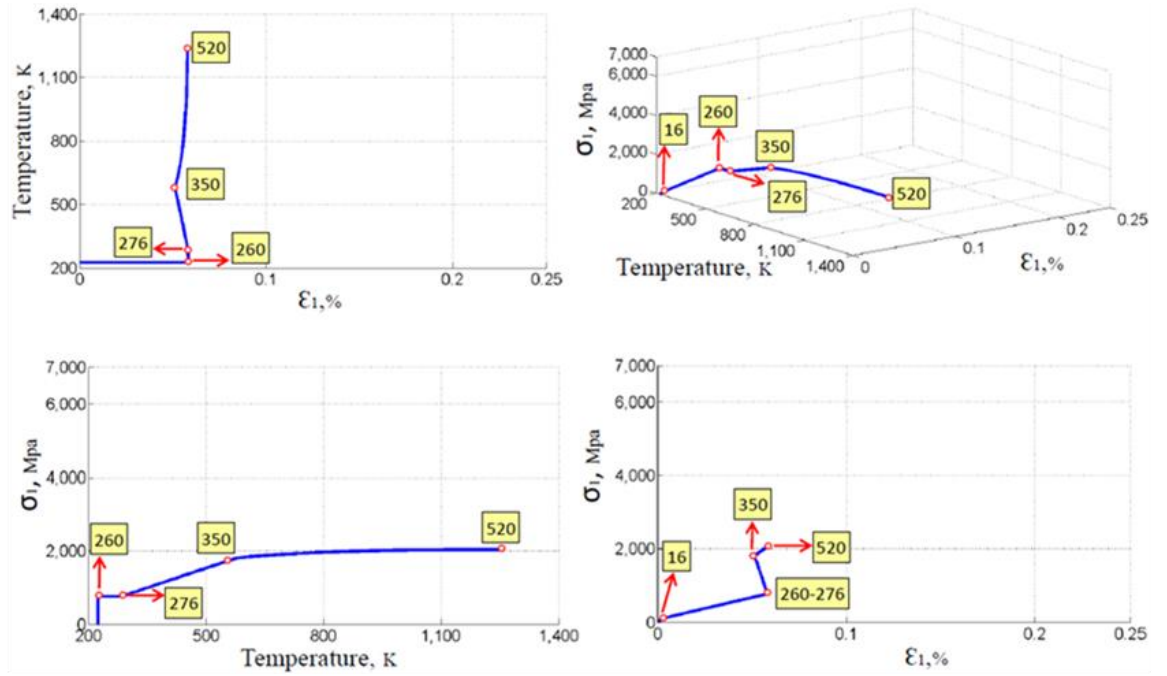

Figure 4.17: Principal stress, principal strain at point 3 for 6.5% strain

Figure 4.18 presents the contour plots of transformation strain for the second geometry variation (B1,B2) as well as the base specimen for loading levels 6.5%, 8.5%, and 10.7% strain at the end of load step 1. In all the specimens, if the transformation strain is 0, the material at that region is considered to be in twinned martensite phase. If the transformation strain is equal to the maximum value of transformation strain than the material phase is considered to be pure detwinned martensite. If the value of transformation strain is between zero and the maximum value of transformation strain than, the material is considered to be mixture of twinned and detwinned martensite.

From the Figure 4.18, it is observed that the transformation strain is maximum at a point on the notch which is away from stress concentration point. This is because at these points the shear strain is maximum and the transformation strain is related to deviatoric components. In case 1, the transformation strain is maximum between the notches and as the notches are shifted horizontally the transformation strain path changes. When the transformation strains are compared for base, B1 and B2 specimens; the maximum transformation strain in load step 1 is 0.191682 observed in case 3.

While holding the specimen in tension the specimen is heated uniformly in the load step 2. The transformation strain contour plots at the end of load step 2 for different displacements are shown in Figure 4.19. From the literature it is learnt that when the material is in detwinned martensite phase and is heated, at a certain temperature the material transforms to austenite phase. By the same principal, in this work when the specimen is heated, the material transforms to austenite phase. At higher temperatures the austenite phase is stable, hence it is considered to be as the parent phase. At higher loads and higher stresses the material phase transforms to detwinned martensite phase thus it is considered to be product phase. Hence when compared with the literature the results can be quantified as, if the magnitude of transformation strain is 0 the material is in austenite phase. If magnitude of transformation strain is maximum, then the phase is in detwinned martensite phase. If the value of transformation strain is between 0 and the maximum transformation strain, the material is considered to be mixture of twinned martensite, detwinned martensite and austenite. It is observed that the magnitude of transformation strain decreases in load step 2. This is the indication that the material phase is transforming to austenite

phase. The magnitude of transformation strain decreases in load step 2. The maximum transformation strain at the end of load step 2 is observed in case 3.

From the Figure 4.19, it can also be interpreted that with the notched away to each other a there is no transformation observed. Hence we can conclude that with the change in the notch sizes, the material6 phases around the notches and in the specimen can be changed.

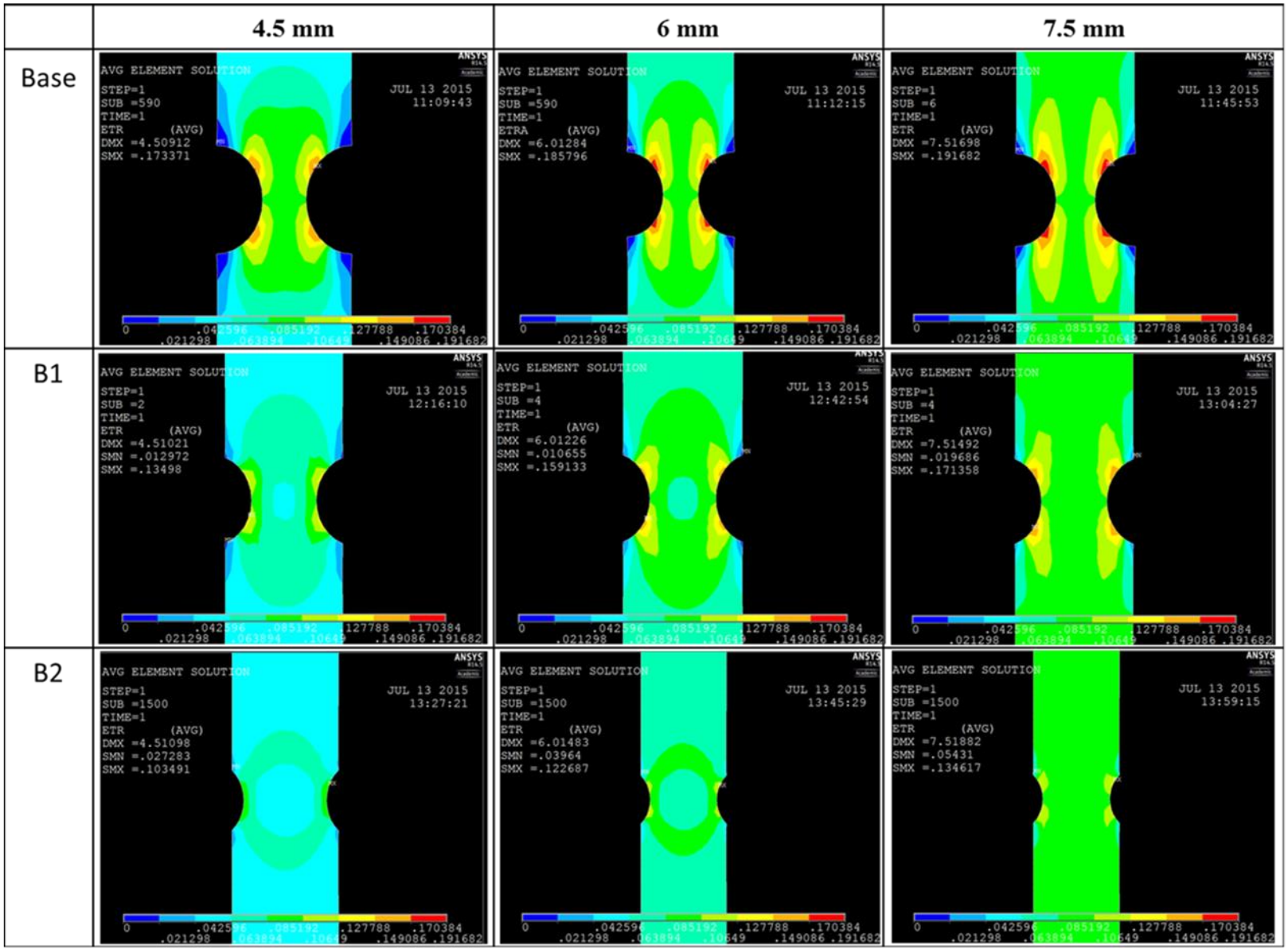

Figure 4.18: Contour plots of transformation strain for base, B1 and B2 specimens at end of load step 1

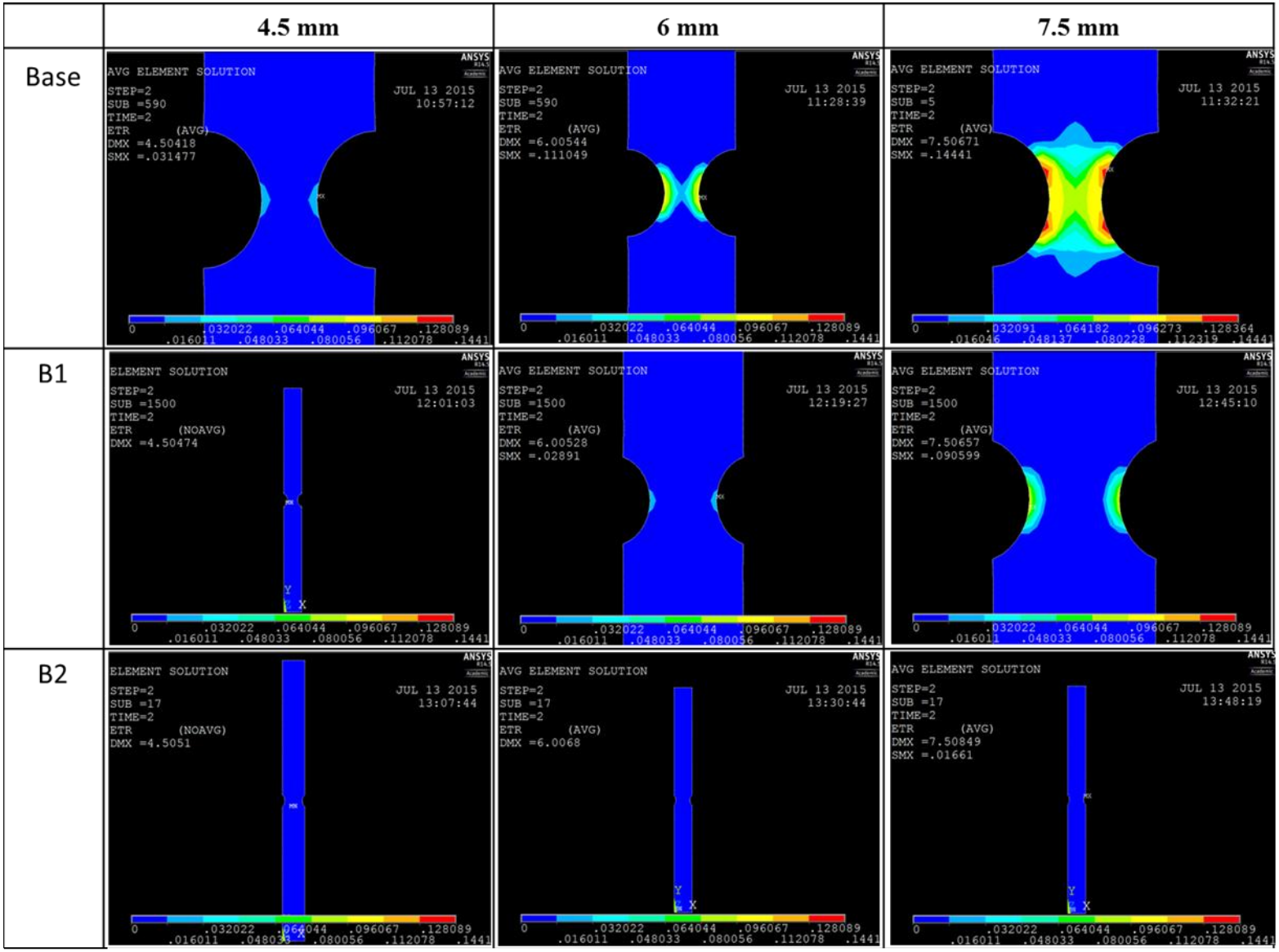

Figure 4.19: Contour plots of transformation strain for base, B1 and B2 specimens at end of load step 2

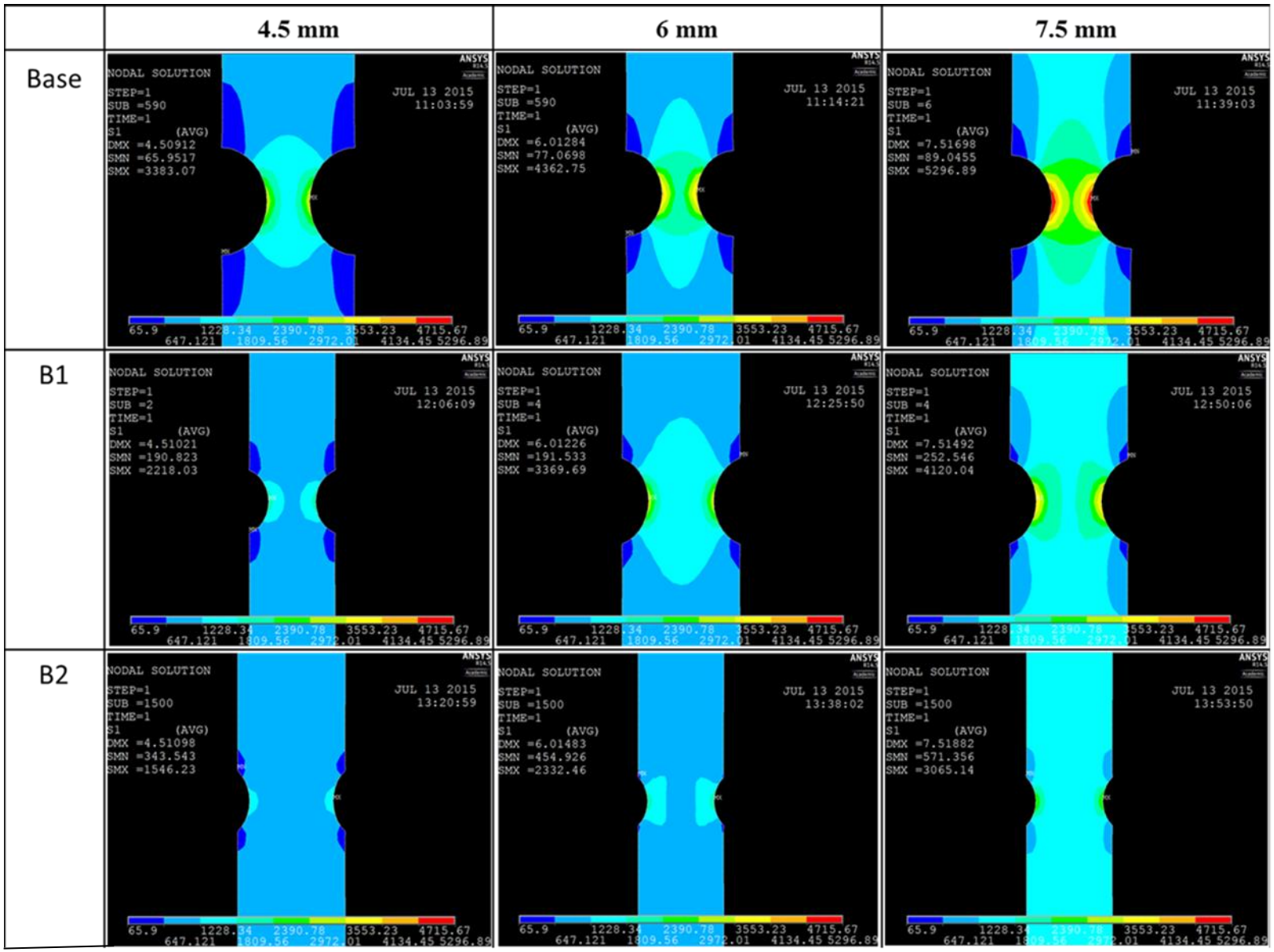

Figure 4.20: Contour plots of Principal stress for base, B1 and B2 specimens at end of load step 1

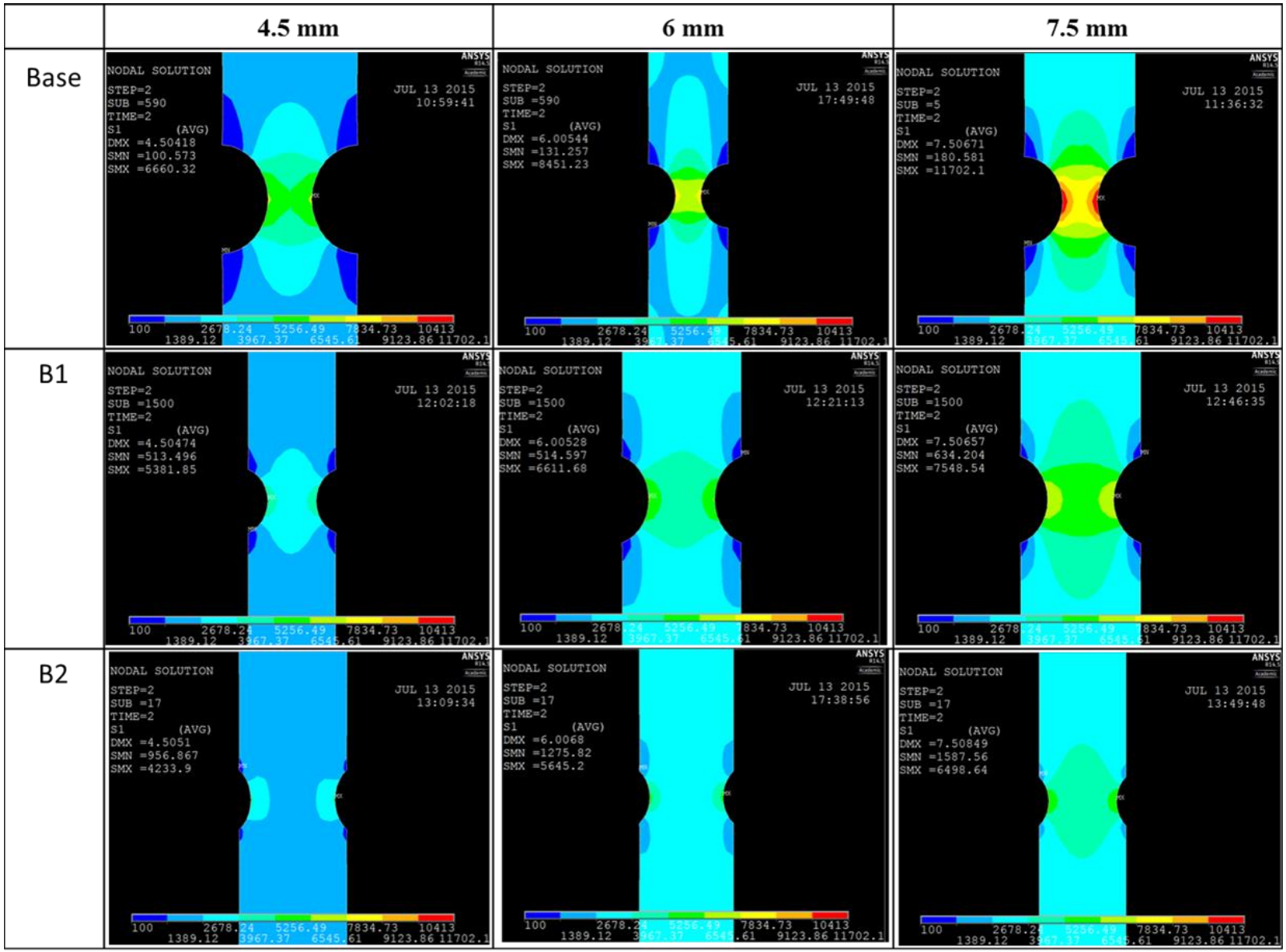

Figure 4.21: Contour plots of Principal stress for base, B1 and B2 specimens at end of load step 2

Figure 4.20 presents the contour plots of 1st principal stresses for base, B1 and B2 specimens at end of load step 1. The maximum 1st principal stress is 5296.89 MPa, is observed at the stress concentration area for case and the minimum 1st principal stress is 65.9 MPa and is observed for case 3. For the base specimen as the displacement increases, the magnitude of maximum principal stress and the minimum principal stress increases. The principal stresses are related to the shear stress and the other combined stresses in the specimen.

When all the contour plots at end of load step 2 are compared, the maximum principal stress is 11702.1 MPa and the minimum principal stress is 100 MPa. It is almost double the value of principal stress in load step 1. This is because, when the specimen is heated the material transforms to austenite. The crystal structure of austenite is cubic structure lattice, which occupies less volume than the orthorhombic crystal structure of detwinned martensite. In austenite phase the specimen tries to shrink. But, since the specimen is constrained, the structure is not able to shrink. Due to this high stresses are generated in the specimen; which can be explained in Figure 4.21. Since the non-uniform distribution of material phases is estimated only analytically, these results must be validated with the experimental results.

The contour plots of transformation strain and 1st principal stress for all the specimens considered show a wide range of phase distribution and stress levels. As expected, increased applied displacement produces larger stresses, at the end of both load steps. Slightly eccentric double notch case (Case 6) produces the highest stresses; this specimen would be most likely to fail first among all others considered. Due to fracture toughness of martensite phase being much lower than that of the austenite phase, the crack is expected to follow a path rich in martensite phase. The phase maps constructed in this chapter for the various double notch specimens are complex, and at times may not be produce intuitive results. In order to provide further understanding on how the phases are evolving under combined mechanical and thermal loading conditions, three additional problems involving simple rectangular geometries are considered in Appendices H, I and J.

CHAPTER 5 Conclusions and Future Work

5.1 Conclusions

SMAs can be utilized as actuators serving as release mechanisms for enclosure gates. Their unique thermo-mechanical behavior in recovering shape upon heating, and being able to tolerate large deformations without undergoing plastic transformations make them potentially good choices for actuators. The failure and fracture of SMAs are the focus of this study; controlled failure is the overarching goal, which requires accurate prediction of stress fields at different stages of deformation. Also, the material properties differ significantly between martensite and austenite phases. Hence, knowledge of phase distribution in a single specimen is critical for accurate fracture predictions. Following the formulation by Souza et al [27], transformation strain can be used for identification of different phases present in a specimen at different stages of deformation.

In this work, a finite element analysis software tool, ANSYS, is used to numerically calculate the transformation strain. A two-dimensional model of Cu-Al-Zn-Mn shape memory alloy specimen is considered in the analysis. The material phases in SMA are estimated by the magnitude of the transformation strain, which is not a standard output quantity. The specimen undergoes a nontraditional loading path that involves two load steps. The results are in the form of contour plots of transformation strain and 1^{st} principal stress at the end of each load step. The

behaviors of the transformation strain and 1st principal stress are also studied for different geometric configurations.

This study demonstrated a method for mapping the non-uniform distribution of material phase in an arbitrarily shaped specimen under combined mechanical and thermal loading. It has been shown that by adjusting specific features of the specimen geometry and loading conditions a wide range of non-uniform phase maps can be obtained. Since the mechanical properties (elastic modulus, yield strength and ultimate strength) of the material with different phases are expected to differ shown in (Table 1.1), actuators of specific breaking patterns can be designed utilizing the methods explained in this work.

5.2 Future Work

This work can be continued in different directions;

i. Since non-uniform distribution of material phases are estimated analytically, this theory has to be verified with series of experiments. An experiment has to be designed in which the specimen has to first undergo tensile loading, then while being held, it should be heated above the austenite finish temperature (A_f). This experiment has to be conducted for different loads and different geometric configurations used in the present work. The experimental results should be then compared with the analytical results.
ii. Since the material phases are estimated, the fracture mechanics has to be studied for different phases. Since the problem is on controlled failure, the fracture toughness and the stress intensity factors should be estimated for martensite, austenite and in the mixed phases at different loads and temperatures.
iii. The phase map should be studied on specimens of different geometries e.g. single notch or triple notch specimens and 3-d geometry. This would improve the current capability and may lead to further applications of the technology.

iv. The plasticity model should be used in the future studies and the behavior of the transformation strain with yielding has to be studied. In the present work, the yield stress and the fracture of the material are not considered.

List of References

1. Kumar. P. K., Lagoudas. D. C: “Introduction to Shape Memory Alloys. In Shape Memory Alloys”. Springer US: 2008. Vol. 1, pp 1-51.
2. http://www.hk-phy.org/iq/memory_alloy/memory_alloy_e.html
3. Lexcellent, Christian: “Shape Memory Alloys Handbook”. John Wiley & Sons. 2013.
4. Buehler. W. J, Gilfrich. J. V, Wiley. R. C: “Effect of Low-Temperature Phase Changes on the Mechanical Properties of Alloys near Composition TiNi”. Journal of Applied Physics 1963. 34 (5), 1475-1477.
5. Wang. F. E, Buehler. W. J, Pickart. S. J: “Crystal Structure and a Unique Martensitic Transition of TiNi”. Journal of Applied Physics. 1965, 36 (10).
6. Wayman. C. M, Harrison. J. D: “The Origins of The Shape Memory Effect”. Journal of the Minerals Metals & Materials Society. 1989, 41 (9), 26-28.
7. Duerig, Pelton : “TiNi Shape Memory Alloys, Materials Properties Handbook Titanium Alloys”. 1994, 1035-1048.
8. Barbarino. S, Flores. E. I. S, Ajaj. R. M, Dayyani. I, Friswell. M. I: “A review on shape memory alloys with applications to morphing aircraft”. Smart Materials and Structures 2014, 23 (6).
9. Lorenza. P, Francesco. M: “Biomedical Applications of Shape memory alloys”. Journal of Metallurgy, 2011.
10. Machado. L. G, Savi. M. A: “Medical applications of shape memory alloys”. Brazilian Journal of Medical and Biological Research. 2003, 36: 683-691.
11. Pelton, Stoeckel, Dueri: “Medical Uses of Nitinol”. Material Science Forum, Vols. 327-328, 63-70.
12. Vajreshwari. U, Venkataramana. K, Reddy. G, Rajeev. V: “Applications of Dampers for Vibration Control Of Structures: An Overview”. International Journal of Research in Engineering and Technology, 2013.

13. Patoor. E, Eberhardt. A, Berveiller. M: “Thermo-mechanical Behavior of Shape Memory Alloys”. Archives of Mechanics. 1988, 40 (5-6), 775-794.
14. Patoor. E, Eberhardt. A, Berveiller. M: “Micromechanical modelling of superelasticity in shape memory alloys”. Journal De Physique. 1996, 6 (C1), 277-292.
15. Sun. Q. P, Hwang. K. C: “Micromechanics modelling for the constitutive behavior of polycrystalline shape memory alloys — II. Study of the individual phenomena”. J. Mech. Phys. Solids. 1993, 41 (1), 19–33.
16. Gao. X, Huang. M and Catherine Brinson. L: “A multivariant micromechanical model for SMAs Part 1. Crystallographic issues for single crystal model”. International Journal of Plasticity. 2000 (16), 1345 – 1369.
17. Boyd. J. G, Lagoudas. D. C: “A thermo-dynamical constitute model for shape memory materials. The monolithic shape memory alloy”. International Journal of Plasticity. 1996, 12 (6), 805-842.
18. Tanaka. K: “A Thermo-mechanical Sketch of Shape Memory Effect - One-Dimensional Tensile Behavior”. Res Mechanica. 1986, 18 (3), 251-263.
19. Qidwai . M. A, Lagoudas .D . C: “On thermo-mechanics and transformation surfaces of polycrystalline shape memory alloy materials”. International Journal of Plasticity. 1999.
20. Yi. S, Gao. S: “Fracture toughening mechanism of shape memory alloys due to martensite transformation”. International Journal of Solids Structure 2001, 38 (24–25) : 4463–76.
21. Auricchio. F, Taylor. R. L: “Computational Methods of Applied Mechanical Engineering”. 1997, 143:175–94.
22. McMeeking. R. M, Evans. A. G:”Mechanics of Transformation-Toughening in Brittle Materials”. Journal of the American Ceramic Society. 1982, 242- 246.
23. Wang. G. Z: “Effects of notch geometry on stress-strain distribution, martensite transformation and fracture behavior in shape memory alloy NiTi”. Materials Science and Engineering Structural Materials Properties Microstructure and Processing. 2006, 434 (1-2), 269-279.
24. Baxevanis. T, Chemisky. Y, Lagoudas. D. C: “Finite element analysis of the plane strain crack-tip mechanical fields in pseudoelastic shape memory alloys”. Smart Materials and Structures. 2012, 21 (9).

25. Victor Birman: “On mode I fracture of shape memory alloy plates”. Smart Material Structure. 1998, (7) 433.
26. Waram. T. C: “Actuator Design Using Shape Memory Alloys”. Ontario Press, 1993, Canada.
27. Angela C. Souza, Edgar N. Mamiya, Nestor Zouain: “Three-dimensional model for solids undergoing stress-induced phase transformations”. Eur. J. Mech. A/Solids I7 (1998), 789-806.
28. DesRoches. R, Delemont. M: “Seismic retrofit of simply supported bridges using shape memory alloys”. Engineering structures. 2002 (24), 325-332.
29. Hartl. D. H and Lagoudas. D. C: “Thermomechanical Characterization of Shape Memory Alloy Materials”. Springer US. 2008, Vol. 1, pp 54-112.
30. Janke. L, Czaderski. C, Motavalli. M, Ruth. J: “Applications of shape memory alloys in civil engineering structures - Overview, limits and new ideas”. Materials and Structures. 2005,(38) 578-592
31. Carmine. M, Emanuele. S and Franco. F: “Crack tip stress distribution and stress intensity factor in shape memory alloys”. Fatigue &Fracture Engineering Materials & Structures. 2013
32. Auricchio. F: “A Robust Integration-Algorithm for a Finite-Strain Shape-Memory-Alloy.” International Journal of Plasticity. 17 (2001): 971-990.
33. Auricchio. F, Taylor. R. L, Lubliner. J: “Shape-Memory Alloys: Macromodeling and Numerical Simulations of the Superelastic Behavior.” Computational Methods in Applied Mechanical Engineering. 146, 1 (1997): 281-312.
34. Sittner. P, Hara. H, Tokuda. M: “Experimental study on the thermoelastic martensitic transformation in shape memory alloy polycrystal induced by combined external forces.” Metall. Mater. Trans. A, 26A, (1995): 2923-2935.
35. Daly. S, Miller. A, Ravichandran. G, Bhattacharya. K: “An experimental investigation of crack initiation in thin sheets”. Acta Materilia. 55 (2007): 6322-6330.

APPENDIX A

ABBREVIATIONS

SMAs	Shape Memory Alloys
HTSMAs	High Temperature Shape Memory Alloys
NOL	Naval Ordinance Laboratory
SME	Shape Memory Effect
SAMPSON	Smart Aircraft and Marine Propulsion Sydtem
SIF	Stress Intensity Factor
CT	Compact Tension
DSC	Differential Scanning Calorimetry
FEA	Finite Element Analysis

APPENDIX B

SYMBOLS

M_s	Martensite start temperature
M_f	Martensite finish temperature
A_s	Austenite start temperature
A_f	Austenite finish temperature
σ_s	Detwinning start stress
σ_f	Detwinning finish stress
σ^{Ms}	Minimum stress at which martensite phase starts
σ^{Mf}	Minimum stress at which martensite phase finishes
σ^{As}	Minimum stress at which austenite phase starts
σ^{Af}	Minimum stress at which austenite phase finishes
C^A	Slope of austenite transformation surface in stress-temperature plot
C^M	Slope of martensite transformation surface in stress-temperature plot
ε	Total strain in the material
ε_e	Elastic strain in the material
ε_T	Transformation strain in the material
e	Deviatoric strain tensor
T	Cauchy stress tensor
S	Deviatoric stress tensor

ξ_s	The value of transformation strain in detwinned martensite phase
λ, μ	Lamé constants
h	Material parameter related to hardening of the material during phase transformation
$\tau_M(\theta)$	Material parameter which defines the positive function of the temperature θ
D^{mech}	Mechanical dissipation inequality defined in terms of internal entropy of the material
R	Elastic region radius in the phase transformation
ε_Z	Strain in z- direction
γ_{XZ}	Shear strain in xz direction
γ_{YZ}	Shear strain in yz direction
τ_{XZ}	Shear stress in xz direction
τ_{YZ}	Shear stress in yz direction
U_x	Displacement in x direction
U_y	Displacement in y direction
$\|\|\boldsymbol{e}_T\|\|$	Magnitude of transformation strain
$\|\|\boldsymbol{e}_{tot}\|\|$	Magnitude of total strain tensor
$\|\|\boldsymbol{e}_{el}\|\|$	Magnitude of elastic strain tensor

APPENDIX C

ANSYS INPUT FILE FOR BASE SPECIMEN FOR 10.7 % strain

```
fini
/clear,all,all
/FILNAME, 75di
/prep7
ET,1,182
keyopt,1,3,2
Mp,ex,1,30.7e3
Mp,nuxy,1,0.36
c1=9230
c2=253.15
c3=73.4
c4=4.2
c5=0.1
c6=30.7e3
c7=0
Tb,sma,1,,7,meff
Tbdata,1,c1,c2,c3,c4,c5,c6,c7
K,1,0,0
K,2,6,0
K,3,6,70
K,4,0,70
```

k,5,3,0

k,6,3,70

k,7,6,35

k,8,0,35

k,9,0,0

k,10,0,70

k,11,0,0

k,12,6,0

Type,1

Mat,1

L,1,2

L,2,3

L,3,4

L,4,1

l,9,5

l,5,6

l,6,10

l,10,9

l,11,12

l,12,7

l,7,8

l,8,11

A,1,2,3,4

a,9,5,6,10

a,11,12,7,8

kwpave,8

pcirc,2,0,360,0

```
kwpave,7
pcirc,2,0,360,0
aovlap,all
adele,6,7,1,0
adele,10,,1,0
adele,8,9,1,0
adele,11,,1,0
esize,0.4
amesh,all
Nsel,s,loc,x,0
Nsel,r,loc,y,0
D,all,all
Nsel,s,loc,y,0
D,all,uy
allsel,all
bfunif,temp,225
Finish
/solu
nropt,unsym
outres,all,all
AUTOTS,on
Solcontrol,1
time,1
Nsel,s,loc,y,70
D,all,uy,7.5
Nsel,all
Solve
```

time,2

bfunif,temp,1250

nsel,all

Solve

finish

APPENDIX D

ANSYS INPUT FILE FOR A1 SPECIMEN FOR 10.7% strain

```
fini
/clear,all,all
/FILNAME, 75di
/prep7
ET,1,182
keyopt,1,3,2
Mp,ex,1,30.7e3
Mp,nuxy,1,0.36
c1=9230
c2=253.15
c3=73.4
c4=4.2
c5=0.1
c6=30.7e3
c7=0
Tb,sma,1,,7,meff
Tbdata,1,c1,c2,c3,c4,c5,c6,c7
K,1,0,0
K,2,6,0
K,3,6,70
```

K,4,0,70

k,5,0,0

k,6,6,0

k,7,6,33

k,8,0,33

k,9,0,37

k,10,6,37

k,11,6,70

k,12,0,70

Type,1

Mat,1

L,1,2

L,2,3

L,3,4

L,4,1

l,5,6

l,6,7

l,7,8

l,8,5

l,9,10

l,10,11

l,11,12

l,12,9

A,1,2,3,4

a,5,6,7,8

a,9,10,11,12

kwpave,7

pcirc,2,0,360,0

kwpave,9

pcirc,2,0,360,0

aovlap,all

adele,6,7,1,0

adele,10,,1,0

adele,8,9,1,0

adele,11,,1,0

esize,0.4

amesh,all

Nsel,s,loc,x,0

Nsel,r,loc,y,0

D,all,all

Nsel,s,loc,y,0

D,all,uy

allsel,all

bfunif,temp,225

Finish

/solu

nropt,unsym

outres,all,all

!Nsubst,1080,1080,1080

autots,on

solcontrol,1

time,1

Nsel,s,loc,y,70

D,all,uy,7.5

Nsel,all

Solve

time,2

bfunif,temp,1250

nsel,all

Solve

Finish

APPENDIX E

ANSYS INPUT FILE FOR A2 SPECIMEN FOR 10.7%

```
fini
/clear,all,all
/FILNAME, 75di
/prep7
ET,1,182
keyopt,1,3,2
Mp,ex,1,30.7e3
Mp,nuxy,1,0.36
c1=9230
c2=253.15
c3=73.4
c4=4.2
c5=0.1
c6=30.7e3
c7=0
Tb,sma,1,,7,meff
Tbdata,1,c1,c2,c3,c4,c5,c6,c7
K,1,0,0
K,2,6,0
K,3,6,7
```

K,4,0,70

k,5,0,0

k,6,6,0

k,7,6,31

k,8,0,31

k,9,0,39

k,10,6,39

k,11,6,70

k,12,0,70

Type,1

Mat,1

L,1,2

L,2,3

L,3,4

L,4,1

l,5,6

l,6,7

l,7,8

l,8,5

l,9,10

l,10,11

l,11,12

l,12,9

A,1,2,3,4

a,5,6,7,8

a,9,10,11,12

kwpave,7

pcirc,2,0,360,0

kwpave,9

pcirc,2,0,360,0

aovlap,all

adele,6,7,1,0

adele,10,,1,0

adele,8,9,1,0

adele,11,,1,0

esize,0.4

amesh,all

Nsel,s,loc,x,0

Nsel,r,loc,y,0

D,all,all

Nsel,s,loc,y,0

D,all,uy

allsel,all

bfunif,temp,225

Finish

/solu

nropt,unsym

outres,all,all

!Nsubst,1080,1080,1080

autots,on

```
solcontrol,1
time,1
Nsel,s,loc,y,70
D,all,uy,7.5
Nsel,all
Solve
time,2
bfunif,temp,1250
nsel,all
Solve
Finish
```

APPENDIX F

ANSYS INPUT FILE FOR B1 SPECIMEN FOR 10.7% strain

```
fini
/clear,all,all
/FILNAME, 75di
/prep7
ET,1,182
keyopt,1,3,2
Mp,ex,1,30.7e3
Mp,nuxy,1,0.36
c1=9230
c2=253.15
c3=73.4
c4=4.2
c5=0.1
c6=30.7e3
c7=0
Tb,sma,1,,7,meff
Tbdata,1,c1,c2,c3,c4,c5,c6,c7
K,1,0,0
K,2,6,0
```

K,3,6,70

K,4,0,70

k,5,3,0

k,6,3,70

k,7,6,35

k,8,0,35

k,9,0,0

k,10,0,70

k,11,0,0

k,12,6,0

k,13,-0.6666,35

k,14,6.6666,35

Type,1

Mat,1

Mat,1

L,1,2

L,2,3

L,3,4

L,4,1

l,9,5

l,5,6

l,6,10

l,10,9

l,11,12

l,12,7

l,7,8

l,8,11

A,1,2,3,4

a,9,5,6,10

a,11,12,7,8

kwpave,13

pcirc,2,0,360,0

kwpave,14

pcirc,2,0,360,0

aovlap,all

adele,6,7,1,0

adele,8,9,1,0

adele,14,,1,0

adele,15,,1,0

esize,0.4

amesh,all

Nsel,s,loc,x,0

Nsel,r,loc,y,0

D,all,all

Nsel,s,loc,y,0

D,all,uy

allsel,all

bfunif,temp,225

Finish

/solu

```
nropt,unsym
outres,all,all
autots,on
solcontrol,1
time,1
Nsel,s,loc,y,70
D,all,uy,7.5
Nsel,all
Solve
time,2
bfunif,temp,1250
nsel,all
Nsubst,1500,1500,1500
Solve
finish
```

APPENDIX G

ANSYS INPUT FILE FOR B2 SPECIMEN FOR 10.7% strain

```
fini
/clear,all,all
/FILNAME, 75di
/prep7
ET,1,182
keyopt,1,3,2
Mp,ex,1,30.7e3
Mp,nuxy,1,0.36
c1=9230
c2=253.15
c3=73.4
c4=4.2
c5=0.1
c6=30.7e3
c7=0
Tb,sma,1,,7,meff
Tbdata,1,c1,c2,c3,c4,c5,c6,c7
K,1,0,0
K,2,6,0
K,3,6,70
```

K,4,0,70

k,5,3,0

k,6,3,70

k,7,6,35

k,8,0,35

k,9,0,0

k,10,0,70

k,11,0,0

k,12,6,0

k,13,-1.3333,35

k,14,7.3333,35

Type,1

Mat,1

Mat,1

L,1,2

L,2,3

L,3,4

L,4,1

l,9,5

l,5,6

l,6,10

l,10,9

l,11,12

l,12,7

l,7,8

l,8,11

A,1,2,3,4

a,9,5,6,10

a,11,12,7,8

kwpave,13

pcirc,2,0,360,0

kwpave,14

pcirc,2,0,360,0

aovlap,all

adele,6,7,1,0

adele,8,9,1,0

adele,14,,1,0

adele,15,,1,0

esize,0.4

amesh,all

Nsel,s,loc,x,0

Nsel,r,loc,y,0

D,all,all

Nsel,s,loc,y,0

D,all,uy

allsel,all

bfunif,temp,225

Finish

/solu

nropt,unsym

outres,all,all

Nsubst,1500,1500,1500

time,1

Nsel,s,loc,y,70

D,all,uy,7.5

Nsel,all

Solve

time,2

bfunif,temp,1250

nsel,all

AUTOTS,on

Solcontrol,1

Solve

finish

APPENDIX H

Case-1

In order to demonstrate the current approach's ability to identify phases and phase mixtures in the specimen due to the combination of stress and temperature conditions, a simple problem involving a 2-D rectangle specimen with dimensions of 6 mm X 70 mm is considered. The material properties of Cu-Al-Zn-Mn SMA are used. The boundary conditions are:

i. U_X (x=0, y) = 0
ii. U_Y (x, y=0) = 0

The 2-D Plane 182 quadrilateral elements are used for meshing. Initially the specimen is cooled to 225ºK. Two load steps are used to solve the problem. In load step 1, a displacement loading is applied in tensile direction on the top surface of the specimen; the displacement is ramped up linearly with the number of sub-steps. In the load step 2, while holding the specimen at constant displacement, a uniform temperature increase of 1025 $^{\circ}$K (from 225 $^{\circ}$K to 1250 $^{\circ}$K) is applied. The total numbers of sub-steps used in each load step are 320. In this case 5 different strain levels are considered 6.5%, 8.5%, 10.7%, 12.8% and 15.7%. Figure A-1 represents the variation of the transformation strain and the sub-steps. From the results, it is interpreted that at the end of load step 1 in strain levels 6.5%, 8.5% and 10.7%, the material phase is a mixture of twinned and detwinned martensite. When the strain levels are increased to 12.8% and 15.7%, at the end of load step 1 the material phase transforms to pure detwinned martensite. In load step 2, when the specimen is heated to 1250 $^{\circ}$K, the specimens for all strain levels transform to austenite phase. The detwinning start stress for 5 different strain levels, the detwinning finish stress for 12.8% and 15.7% strain levels, and austenite start and finish stresses and corresponding temperatures for all strain levels can be identified to construct the stress-temperature graph. Figure A-2 shows the stress-temperature plot where detwinning start stress is σ_s = 70.85 MPa and the detwinning

finish stress is σ_f = 1400 MPa. Similarly, the austenite start and finish temperature are found to be A_s = 110 ºK and A_f = 250 ºK respectively.

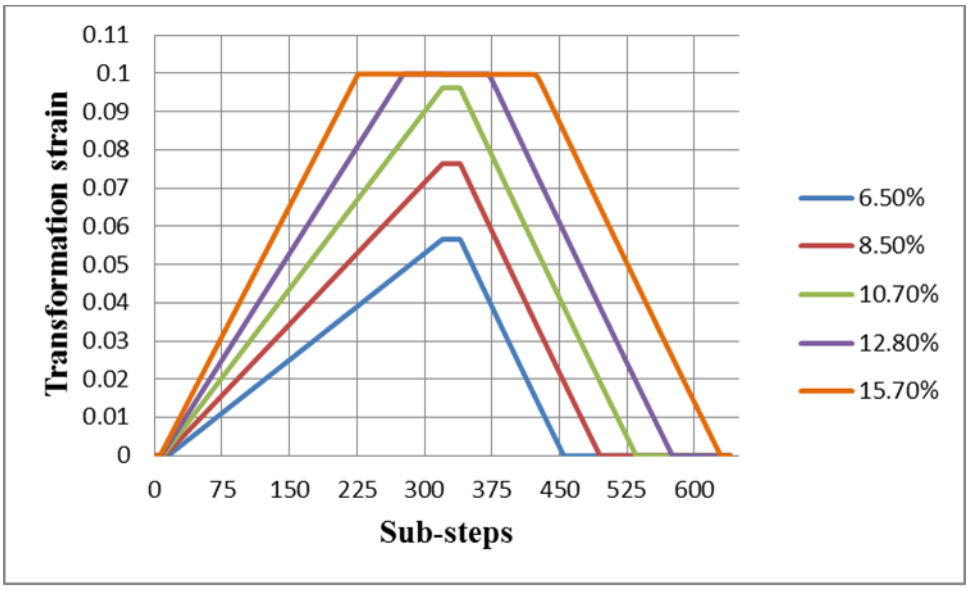

Figure A-1: Transformation strain vs sub-steps.

The progressions of phase transformation for the five cases are clearly observable in Figure A-2. At the end of load step 1, the three final strain cases (6.5%, 8.5% and 10.7%) remain in the mixed twinned/detwinned martensite phase while the 12.8% and 15.7% final strain cases surpass the detwinning finish stress σ_f. Upon applying the temperature increase in a ramped fashion in load step 2, the 6.5%, 8.5% and 10.7% strain cases exhibit stress increase until they reach the stress-temperature line that defines the completion to austenite transformation. During the load step 2, 12.8% and 15.7% final strain cases remain at the constant stress level until the temperature reaches the austenite transformation start line; at this point, the stress starts increasing with temperature increase until the transformation is complete.

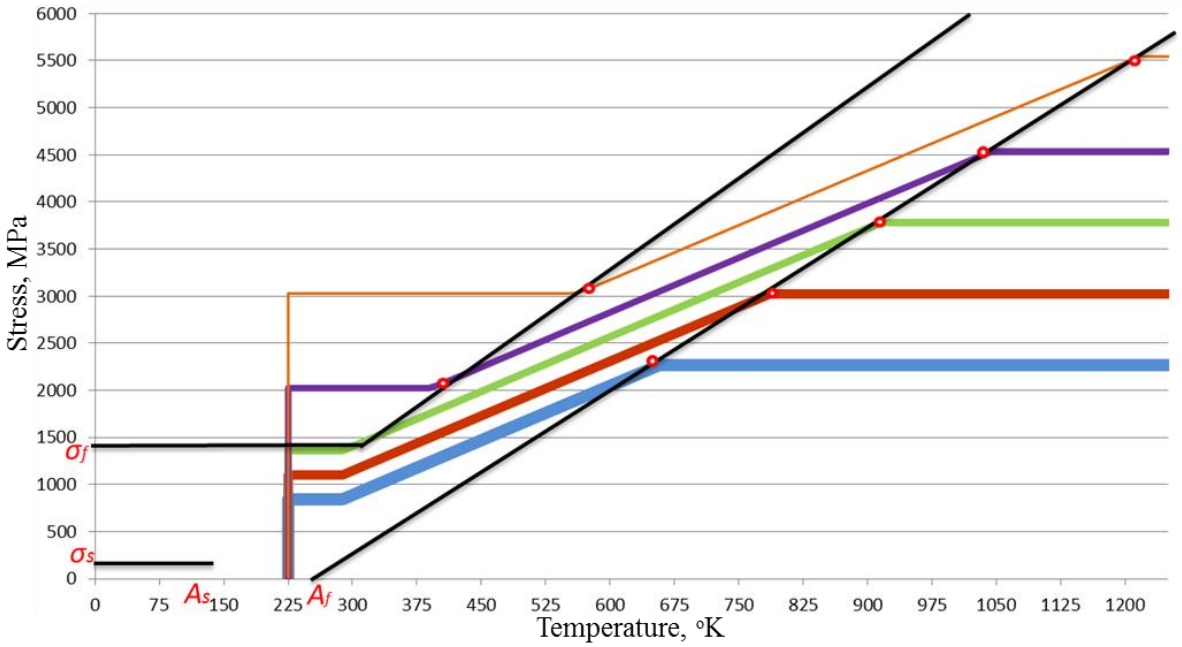

Figure A-2: Stress- temperature plot.

APPENDIX I

Case-2

To demonstrate the current approach's ability to identify phases and phase mixtures in the specimen due to the combination of temperature and stress conditions, another problem involving a 2-D rectangle specimen with dimensions of 6 mm X 70 mm is considered. The material properties of Cu-Al-Zn-Mn SMA are used. The boundary conditions are:

i. U_X (x=0, y) = 0
ii. U_Y (x, y=0) = 0

The 2-D Plane 182 quadrilateral elements are used for meshing. The austenite finish temperature (300 ºK) from APPENDIX F is considered in this approach. Initially the specimen is cooled to 225 ºK. Two load steps are used to solve the problem. In load step 1, the specimen is heated with a uniform temperature, with a uniform increase from 225 $^{\circ}$K to 300 $^{\circ}$K. In load step 2, a displacement loading is applied in tensile direction on the top surface of the specimen. The displacement is ramped up linearly with the number of sub-steps. The total numbers of sub-steps used in each load step are 320. In this study 5 different strain levels are considered 6.5%, 8.5%, 10.7%, 12.*% and 15.7%. Figure A-3 represents the variation of the transformation strain and the sub-steps.

From the results, it is interpreted that at the end of load step 1 in all the strain levels, the material phase is pure austenite. At the end of load step 2 in strain levels 6.5%, 8.5% and 10.7%, the material is a mixture of austenite and detwinned martensite. When the strain levels are increased to 12.8% and 15.7%, at the end of load step 2 the material phase transforms to pure detwinned martensite.

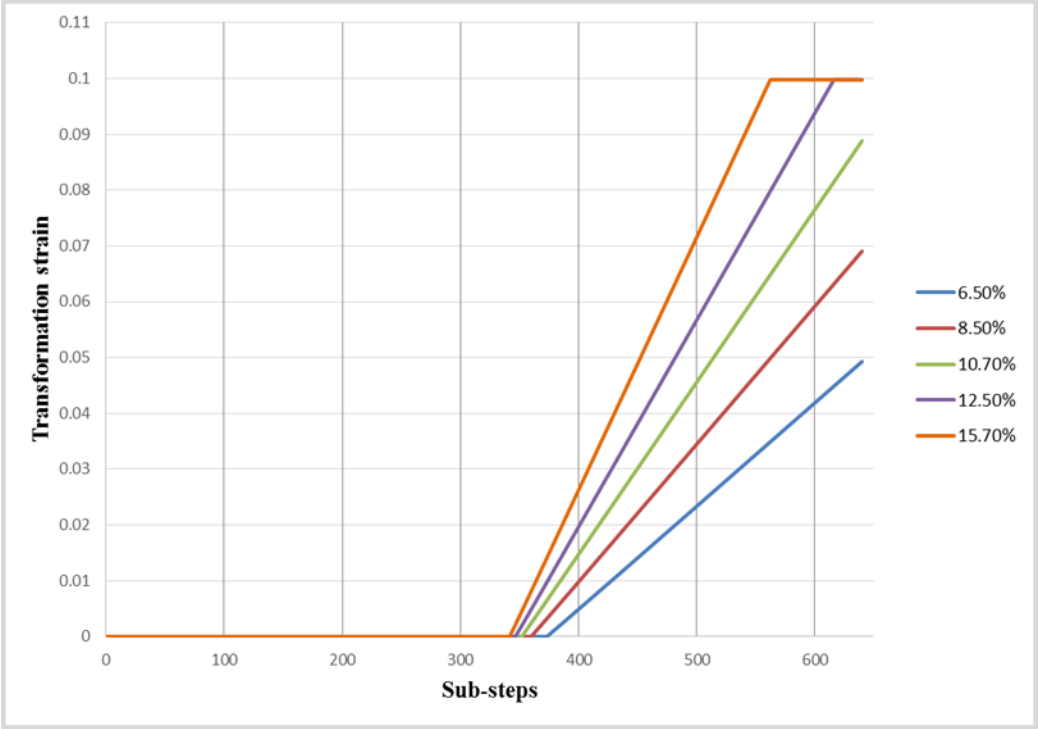

Figure A-3: Transformation strain vs sub-step.

The detwinning start stress for 5 different strain levels, the detwinning finish stress for 12.8% and 15.7% strain levels, can be identified to construct the stress-temperature graph.

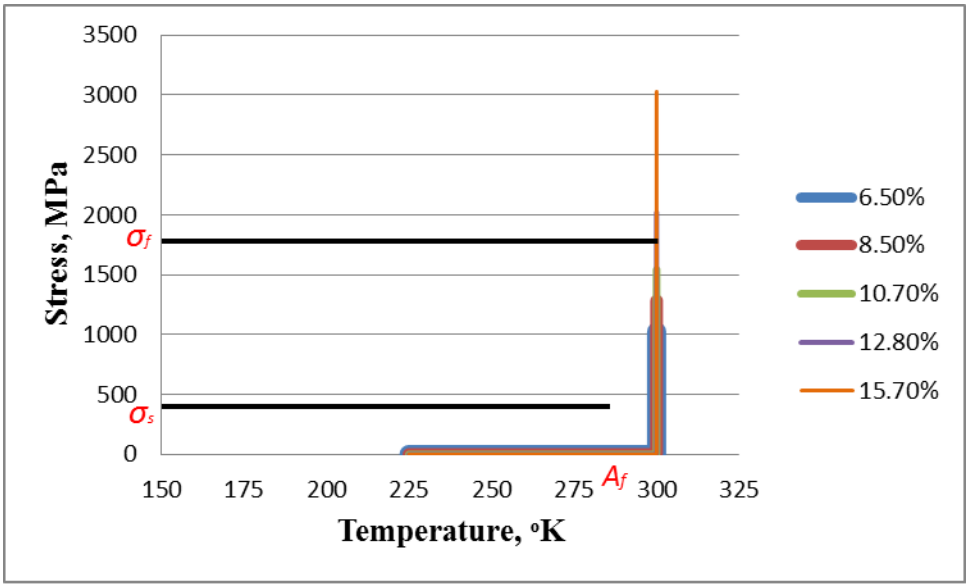

Figure A-4: Stress- temperature plot.

Figure A-4 shows the stress-temperature plot where detwinning start stress is σ_s = 385 MPa and the detwinning finish stress is σ_f = 1680 MPa. The progressions of phase transformation for the five cases are clearly observable in Figure A-4. At the end of load step 1, the five strain cases remain in the austenite phase. Upon applying load, the stress increases in vertical direction due to constant temperature. During the load step 2, 12.8% and 15.7% strain cases surpass the detwinning finish stress σ_f, while the 6.5%, 8.5% and 10.7% strain levels remain in the mixed detwinned martensite and austenite phase.

APPENDIX J

Case-3

In a final step, a square specimen (6 mm X 6 mm) under shear-type loading is considered. Cu-Al-Zn-Mn SMA properties are used. The boundary conditions used are

i. U_X (x=0, y=0) = 0, U_Y (x=0, y=0) = 0

ii. U_Y (x, y=0) = 0, U_Y (x, y=6) = 0

The 2-d Plane 182 quadrilateral elements are used for meshing. Two load steps are used to solve the problem. In load step 1, the top surface of the specimen is incrementally loaded with a displacement in x-direction. In load step 2, the specimen is unloaded incrementally. The transformation strain is calculated at the center point. The problem is solved with 0.5 mm and 1.0 mm displacement.

Figure A-5 shows the transformation strain variation with number of sub-steps. This problem clearly demonstrates the dependence of transformation strain on the shear stress. Consistent with the mathematical model given in Chapter 4, larger shear stress leads to larger transformation strains.

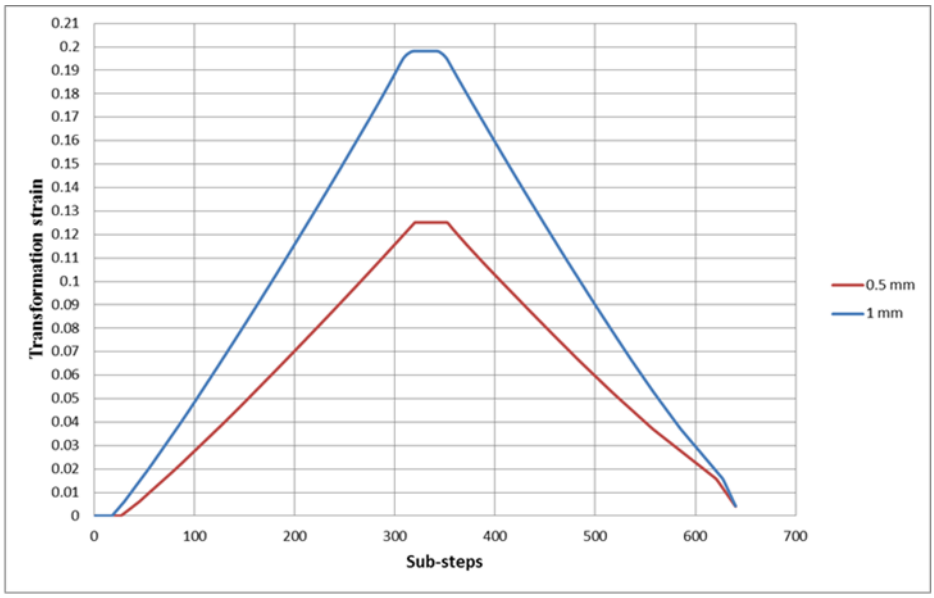

Figure A-5: Transformation strain vs Sub-steps.